5-2014

Selective Oxidations by Metalloporphyrins and Metallocorroles

Tse-Hong Chen
Western Kentucky University, tse-hong.chen137@topper.wku.edu

SELECTIVE OXIDATIONS BY METALLOPORPHYRINS AND METALLOCORROLES

A Thesis
Presented to
The Faculty of the Department of Chemistry
Western Kentucky University
Bowling Green, Kentucky

In Partial Fulfillment
Of the Requirements for the Degree
Master of Science

By
Tse-Hong Chen

May 2014

SELECTIVE OXIDATIONS BY METALLOPORPHYRINS AND METALLOCORROLES

Data Recommended 4-1-14

Dr. Rui Zhang, Director of Thesis

Dr. Eric Conte

Dr. Yan Cao

5-6-14

Dean, Graduate Studies and Research Date

ACKNOWLEDGEMENTS

It is my pleasure to present my appreciation to all the remarkable people who were active parts of my research and made this thesis possible. First of all, I would like to express my deepest gratitude to my research advisor Dr. Rui Zhang for his guidance, patience, advice, encouragement, forgiveness, understanding and moral support to my study at Western Kentucky University and personal experiences in my life. In particular, his kindness and devoted attitude in research guided me greatly. My thesis would not have been successfully completed without his ingenuity and support.

During the course of my study and compilation of the thesis, my sincere thanks go to the following professors and members of my research group who I have worked with and learned from. I am great grateful to have Dr. Eric Conte and Dr. Yan Cao to serve on my thesis committee. Their constructive suggestions, discussions and ideas were very helpful for my future works. In addition, I sincerely thank Dr. Lester Pesterfield for helping in NMR technique, Ms. Alicia McDaniel for helping in chemicals. I would like to thank all my research group members: Zhibo Yuan, Eric Vanover, Helen Thompson, Aaron Carver, Jesse Evans, WeiLong Luo, and Nowelle Altman for their support and assistance, especially, data contributors: Zhibo Yuan, Eric Vanover and Helen Thompson. It is one enjoyable and recallable memory to finish my projects.

This work is supported by a NSF grant (CHE 1213971), and an internal grant from WKU Office of Research (RCAP 2012). Importantly, I am sincerely and supremely appreciated to my parents for their support and love during my study.

Last, I dedicated this thesis to my best friend, Dr. Hsiao-li Chen, who gave me a lot of courage and knowledge during my study at Western Kentucky University and my dearest love, Hsiao-Ting Cheng, who always accompanies me with her spiritual support and happiness.

TABLE OF CONTENTS

LIST OF FIGURES

LIST OF SCHEMES

LIST OF TABLES

SELECTIVE OXIDATIONS BY METALLOPORPHYRINS AND METALLOCORROLES

Tse-Hong Chen May 2014 90 Pages

Directed by: Dr. Rui Zhang, Dr. Eric Conte, and Dr. Yan Cao

Department of Chemistry Western Kentucky University

Highly reactive transition metal-oxo intermediates are important active oxidant involved in numerous enzymes such as cytochrome P450 monooxygenases as well as in many useful metal-catalyzed oxidations. Many transition metal catalysts are designed for biomimetic studies of the predominant oxidation catalysts in Nature, the cytochrome P450 enzymes. In this work, a series of metalloporphyrin and metallocorrole complexes have been successfully synthesized and spectroscopically characterized by UV-vis, GC-MS and ^{1}H-NMR. The utilization of these complexes as catalysts for selective oxidation of sulfides and photocatalytic aerobic oxidations of activated hydrocarbons were investigated.

Ruthenium(II) porphyrin complexes (**2**) and iron(III) corrole complexes (**4**) with iodobenzene diacetate [$PhI(OAc)_2$] as a mild and excellent oxygen source efficiently catalyzed sulfides to sulfoxides under mild conditions. Ruthenium porphyrins (**2**) catalyzed the highly selective oxidation of *para*-substituted thioanisoles and allylic sulfides with $PhI(OAc)_2$ in the presence of visible light. Over 95% conversion and 100% selectivity were achieved within 12 h. Results from competitive catalytic oxidations and spectra studies of the reaction of complexes (**2**) with $PhI(OAc)_2$ in the absence of organic

sulfide showed that the low-reactivity ruthenium(IV)-oxo intermediates (**9**) are most likely to be the active oxidant in the sulfoxidation reactions.

An outstanding method for the highly selective oxidation of sulfides to sulfoxides was developed by using iron(III) corroles (**4**) and $PhI(OAc)_2$ as mild oxygen source. Allylic thioanisoles and hydroxy sulfides could be successfully oxidized with good conversions and excellent selectivities within short time period. A significant accelerating effect on the rate of sulfoxidation reactions by small amount of water was noticed and will be understood by more studies.

Fluorinated diiron(IV) μ-oxo biscorrole complex (**5b**) catalyzes alkenes and activated hydrocarbons using atmospheric oxygen and visible light (sunlight) with up to 1200 TONs. The observed photocatalytic oxidation is ascribed to a photo-disproportionation mechanism to afford a highly reactive corrole-iron(V)-oxo species that can be directly observed by laser flash photolysis methods. It is noteworthy that the use of visible light (solar light) for activation of atmospheric oxygen without the consumption of a reducing agent in aforementioned photocatalysis is particularly relevant to realizing innovative and economically advantageous processes for conversion of hydrocarbons into oxygenates.

1. INTRODUCTION

1.1 Catalytic oxidations of Cytochrome P-450 Enzymes

Catalytic oxidations of organic substrates is of great importance in synthetic organic chemistry and the key to fundamental transformations in Nature.[1] Many fine chemicals, oxygenated compounds and pharmaceuticals to large scale commodities are produced by oxidation reactions and applied worldwide.[2] Traditional oxidation methods often perform with stoichiometric amounts of expensive and/or toxic heavy metals, which generate large amounts of toxic wastes and give low region-, chemo-, enantio- and stereoselectivities.[3-4] The increasing attention of catalytic oxidation processes that employ transition metals as catalysts with environmentally friendly oxygen sources such as molecular oxygen or hydrogen peroxide for selective oxidations is one of the most significant goals in oxidation chemistry.[4-6]

In biological systems, catalytic oxidations facilitated by oxidative enzymes are fundamental in many biosynthesis and biodegradation processes.[7] Most of these biological oxidations are mediated by heme-containing oxygenases. The most prominent of these oxygenases is the ubiquitous cytochrome P450 monooxygenase (CYP450). The cytochrome P450s enzymes transfer one oxygen atom from atmospheric molecular oxygen into a substrate and reduce the second oxygen to water, utilizing reducing agents, such as NADH (nicotinamide adenine dinucleotide) or NADPH (nicotinamide adenine dinucleotide phosphate), as electron donor via electron transport protein systems (Scheme 1).[8] Therefore, cytochrome P450s have been shown to catalyze a wide variety of oxidation reactions in Nature, which include important transformations such as

epoxidation, hydroxylation, dealkylation, dehydrogenation, and oxidation of amines, sulfides, alcohols and aldehydes, many of which are characterized by high degrees of chemo-, regio-, enantio- and stereoselectivities.[7-10] This stimulates enormous efforts in developing biomimetic oxidation catalysts. The most common heme prosthetic group found in heme-containing enzymes is the iron protoporphyrin IX (heme *b*) complex (Figure 1),[8] which is reported as the active site of the oxidation heme-containing enzymes.[7]

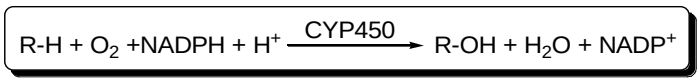

Scheme 1. Monooxygenase reaction.

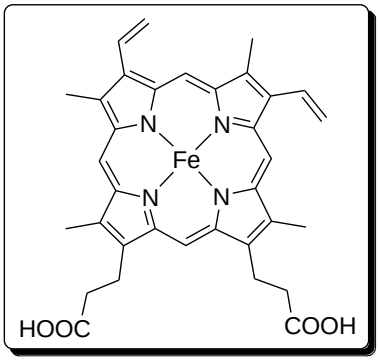

Figure 1. Structure of iron protoporphyrin IX (heme *b*) complex.

The name cytochrome P450 enzymes arises from the reduced protein which efficiently binds carbon monoxide with a strong absorption at 450 nm.[11] The majority of the cytochrome P450s are membrane-bound, associated with the inner mitochondrial and the endoplasmic reticulum of microsomal membranes.[8] The structurally and biochemically best-characterized cytochrome P450s are the soluble camphor-inducible bacterial P-450 monooxygenase ($P450_{cam}$), which was discovered in *Pseudomonas*

putida.[8, 12] The soluble bacterial $P450_{cam}$ is very stable and easy to be purified in large quantities. The enigma of cytochrome P450s structure was deciphered when Poulos et al. provided the first three-dimensional structure of the cytochrome $P450_{cam}$ (Figure 2) in 1986,[13-14] which catalyzes the stereospecific 5-*exo* hydroxylation of the bicyclic terpene camphor with molecular oxygen to 5-*exo*-hydroxycamphor (Scheme 2).[11]

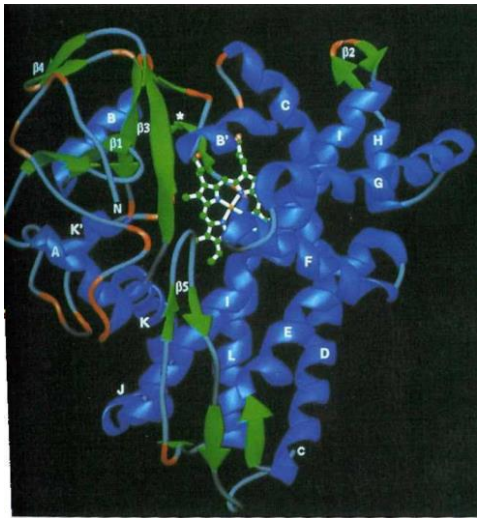

Figure 2. X-ray structure of cytochrome $P\text{-}450_{cam}$.

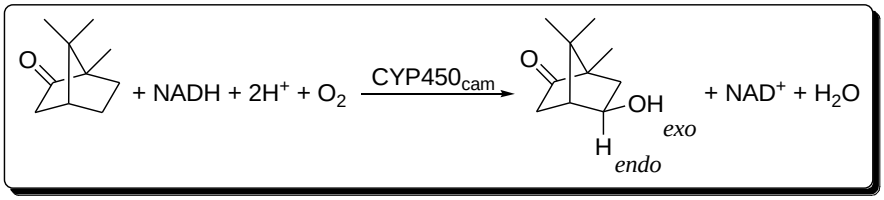

Scheme 2. Stereospecific hydroxylation of the *exo* C-H bond at position 5 of camphor by cytochrome $P450_{cam}$.

As a result of the unique spectral properties as well as the efficiency of the cytochrome P450 enzymes to catalyze a variety of difficult bio-transformations, significant efforts have been directed toward creating artificial mimics of these remarkable enzymes.[4, 9] The active oxidant in the P450 enzyme is usually thought to be

an iron(IV)-oxo porphyrin radical cation, termed as Compound I, by analogy to the intermediates formed in peroxidase and catalase enzymes.[10, 15] In this regard, iron, manganese, and ruthenium transition metals have been employed as substrate-selective catalysts of biomimic models of the cytochrome P450 enzymes.[4, 16] In the past decades, many synthetic metalloporphyrin complexes have been reported as model compounds of heme-containing enzymes and catalysts for a variety of selective oxidation reactions (Scheme 3).[11, 17-18] This study was stimulated by the desire for the better understanding of the intricate mechanisms of biochemical oxidations using simple biomimetic models.

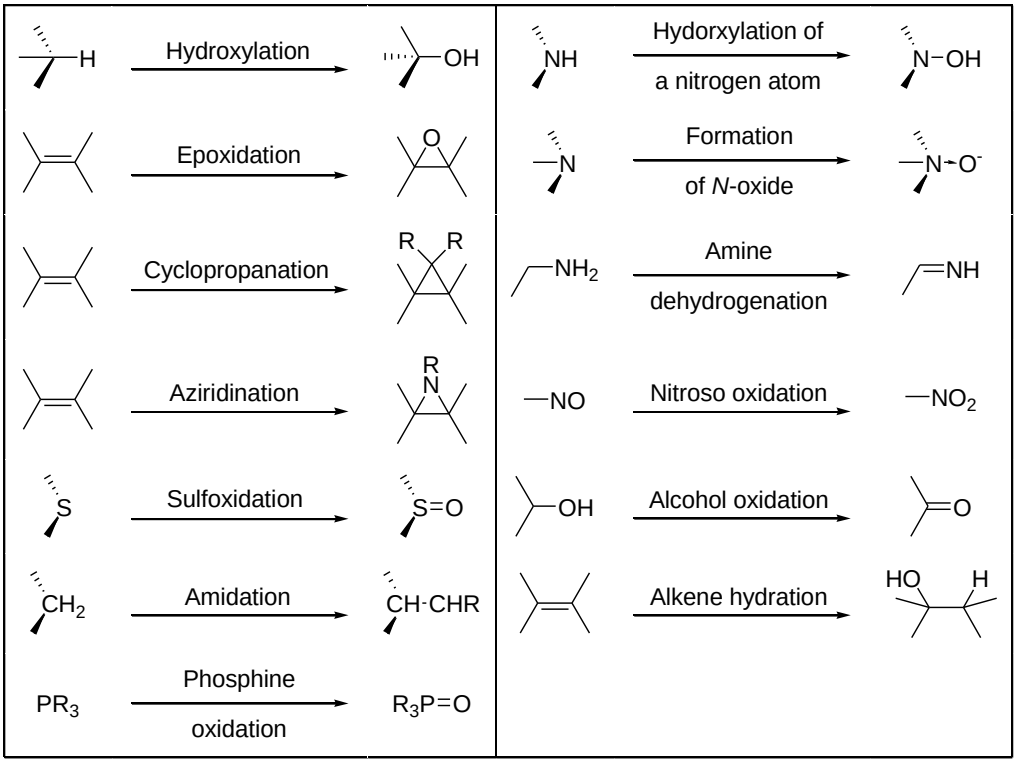

Scheme 3. Typical metalloporphyrin-mediated oxidation reactions.

1.2 Biomimetic models with metalloporphyrins

Metalloporphyrins have been widely used as biomimetic models of cytochrome P450 enzymes to catalyze a variety of oxidation reactions. Groves and co-workers first reported the first oxidation system with a simple iron porphyrin in 1979.[19] This oxidation system, which consists of oxygen source iodosylbenzene and catalyst Fe^{III}(TPP)Cl (TPP = *meso*-tetraphenylporphyrin), catalyzed the effective stereospecific alkene epoxidation and alkane hydroxylation (Scheme 4A). Subsequently, effective catalytic oxidation systems based on metalloporphyrin catalysts with iron, manganese and ruthenium porphyrins with numerous oxygen sources iodosylbenzene, sodium hypochlorite and 2,6-dichloropyridine *N*-oxide have been received current attentions and reported.[4, 11, 20]

High-valent transition metal-oxo species with high reactivity are important active oxidant involved in numerous enzymes such as cytochrome P450 monooxygenases as well as in many useful metal-catalyzed oxidations.[11, 16, 21] High-valent metal-oxo porphyrins have been known as reactive intermediates in the catalytic oxidation cycles and observed in the reactions of synthetic metalloporphyrins with iodosylbenzene, *m*-chloroperbenzoic acid, and molecular oxygen.[4, 6] The first high-valent metal-oxo species, iron(IV)-oxo porphyrin radical cations, has been characterized by oxidation of Fe^{III}(TMP)Cl with *m*-chloroperbenzoic acid at low temperature.[11] In addition, high-valent ruthenium-oxo and manganese-oxo porphyrin intermediates have received considerable attention. Groves and co-workers reported the first manganese(V)-oxo porphyrin complexes in aqueous solution in 1997 which shows unusually high reactivity in olefin epoxidation and alkane hydroxylation.[17, 22]

Ruthenium porphyrins and related complexes attracted intensive attention due to the close periodic relationship to the biologically significant iron. Ruthenium has widest scope of oxidation states from -2 to +8 in various ligand environments.[23] In addition, ruthenium complexes have a variety of useful characteristics including rich coordination, low redox potentials, high electron transfer ability, and stability of reactive metal species.[7] For example, ruthenium porphyrin complexes such as carbonyl ruthenium(II) tetrakispentafluorophenylporphyrin [Ru^{II}(TPFPP)(CO)] efficiently catalyzed the hydroxylation of unactivated alkanes, the cleavage of ethers, and the oxygenation of benzene with 2,6-dichloropyridine *N*-oxide under mild, non-acidic conditions (Scheme 4B).[23]

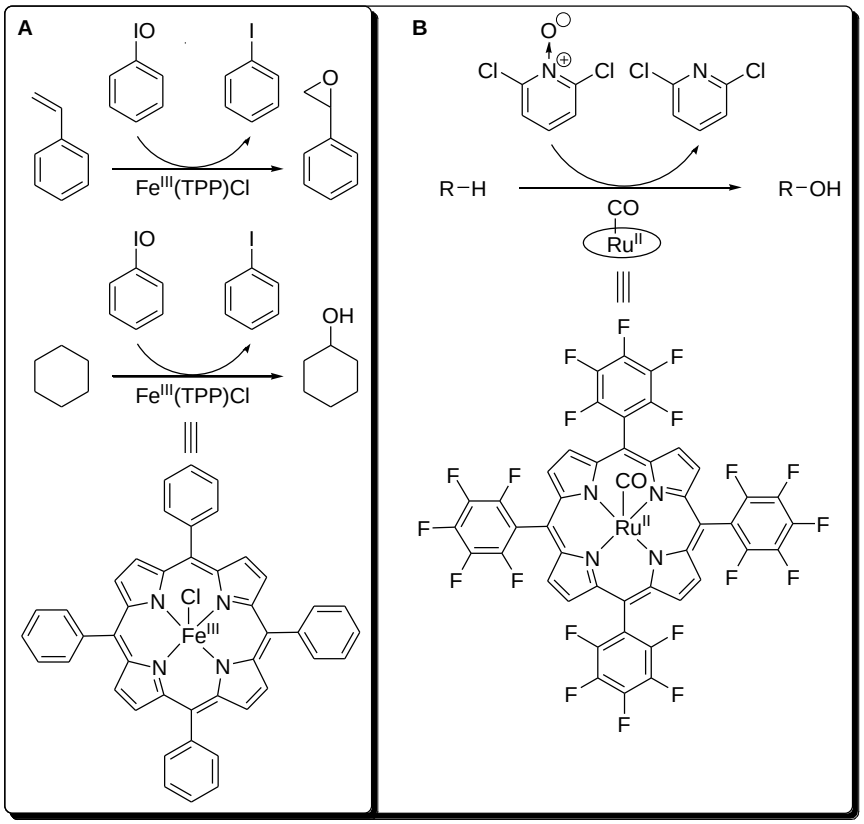

Scheme 4. (A) Alkene epoxidation and alkane hydroxylation catalyzed by Fe^{III}(TPP)Cl. (B) Hydroxylation of hydrocarbons with 2,6-dichloropyridine *N*-oxide catalyzed by Ru^{II}(TPFPP)(CO).

1.3 Biomimetic models with metallocorroles

Corroles are tetrapyrrolic macrocycles, structurally similar to the porphyrin, related to the cobalt-chelating corrin in vitamin B_{12} (Figure 3)[24] and the iron chelating porphyrin in heme. As shown in Figure 4, corrole is the trianionic ligand, which consists of three *meso* carbon positions with a pyrrole-pyrrole linkage and has one imino group and three amino nitrogen groups in the inner core, and, however, porphyrin and corrin are dianionic and monoanionic ligands, respectively. In UV/Vis spectroscopy, corrole shows asymmetric intensely Soret band and weak Q band. Corrole is more acidic than porphyrin,

and easier to form anionic species in basic conditions.[25-26] Moreover, reduced symmetry, a small cavity, and ability to stabilize high-valent transition metal-oxo species result in the increasing attention on corroles and their metal complexes.[27-28] Many novel aspects of the coordination chemistry of corrole-metal complexes have been revealed recently, especially with respect to high metal oxidation states.[29] Furthermore, corrole-metal complexes are expected to be the extensive studies in asymmetric oxidation reaction, photophysics, chemical transformation, and other properties.[30] In recent years, corrole has been focused on *meso*-triaryl-substituted corroles due to a recent progress in its synthesis.[31-32]

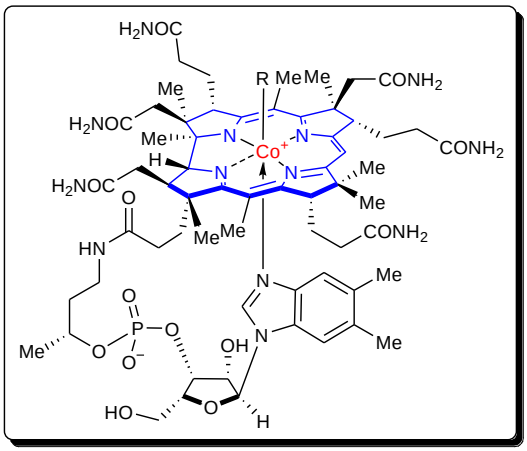

Figure 3. Structure of vitamin B_{12}.

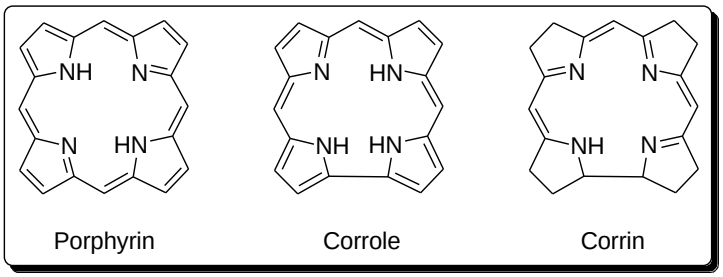

Figure 4. Structure of porphyrin, corrole and corrin.

Johnson and co-workers reported corrole synthesis in 1965 that triggered the corrole chemistry.[25] Hodgkin and co-workers conducted the first crystallography of a free-base corrole in their Vitamin B_{12} project in 1971.[33] Until now, most of reports focused on the synthesis of corroles and investigation of the coordination chemistry of metallocorrole complexes. Comparing to porphyrin systems, reported corrole systems remained sparse.[34-35] Metallocorrole complexes have attracted considerable interest with *meso*-*N*-substituted analogs, namely corrolazines, in view of their similarities to metalloporphyrins.[32, 36-37] The main difference between porphyrins and corroles is π-system of corroles is much more electron-rich than porphyrins[38]. Therefore, trianionic corrolate ligands supports unusually higher metal oxidation states than dianionic porphyrinato ligand. In 1999, Gross and co-coworkers explored a new and efficient synthetic pathway to prepare corroles, i.e. solvent-free condensation of pyrrole and aldehydes under unusual reaction conditions.[32] After the innovative synthesis of corroles, Gross and co-workers first reported utilization of metallocorrole complexes for the catalylytic epoxidation, hydroxylation, and cyclopropanation in the presence of iodosylbenzene and carbenoids (Scheme 5).[39]

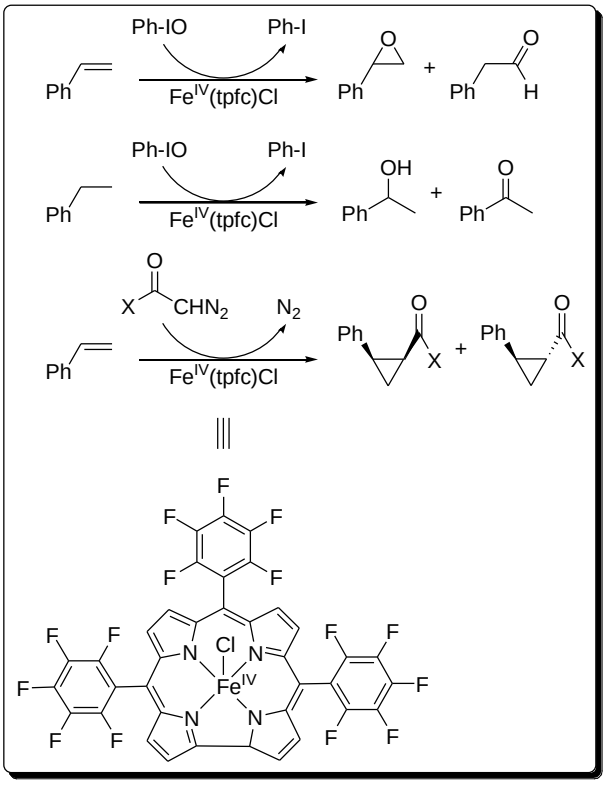

Scheme 5. The catalytic epoxidation, hydroxylation, and cyclopropanation by Fe^{IV}(TPFC)Cl.

Iron is one of the most common metals in the corrole catalysts due to the readily accessible high oxidation state in +4. In catalytic macrocycle-iron-oxo chemistry, the transient with iron in the formal +5 oxidation state exists mainly as an iron(IV)-oxo complex with the ligand oxidized to a radical cation.[40] The well-known porphyrin-manganese(V)-oxo complexes showed higher reactivity than the well-known iron(IV)-oxo radical cation in the same ligand system.[22, 41-42] Species with more highly oxidized iron atoms are rare and a reported iron(V)-oxo complex supported by a tetraanionic ligand showed truly unprecedented reactivity.[43] Zhang and co-workers reported laser flash photolysis generation of high-valent transition metal-oxo species with iron and

manganese. The porphyrin/corrole-iron(V)-oxo transients produced by laser flash photolysis (LFP) methods also displayed the appropriate high level of reactivity.[44-45]

1.4 Sulfoxidation reactions

In biomimetic catalytic oxidations, the selective oxidation of sulfides to sulfoxides (sulfoxidation) is of great importance in organic synthesis.[46] Organic sulfoxides are valuable synthetic reagents for the production of a variety of chemically and biologically significant molecules including carbon-carbon and carbon-oxygen bond formations, cycloaddition reactions, radical addition reactions, molecular rearrangements, functional group transformations and asymmetric catalysis. Optically active sulfoxides are also useful intermediates in medicinal and pharmaceutical chemistry to prepare the therapeutic agents such as antiulcer (proton pump inhibitors), antibacterial, antifungal, antiatherosclerotic, antihypertensive and cardiotonic agents, as well as psychotonics and vasodilators.[47] A large variety of electrophilic reagents such as peracids, hypochlorite, sodium periodate, iodosobenzene, peroxyacids, and highly toxic oxo metal oxidants and hazardous or toxic oxidizing agents have been utilized for the oxidation of conventional sulfides with the aim of obtaining high selectivity for sulfoxide over sulfone, particularly when preparing biologically relevant sulfoxides.[48-49] Therefore, selective oxidation of organic sulfides is the key roles in both industrial and green chemistry because organosulfur compounds are a major source of environmental pollution.

The first synthesis of sulfoxides was reported by Marcker in 1865 and,[46] since then, a variety of reagents and methods have been utilized for this key transformation to the corresponding sulfoxides. However, many methods are either harmful, expensive, or poor selectivity as a result of overoxidation of sulfides to sulfones.[46, 50-52] Based on the

reports by Kowalski and co-workers, hydrogen peroxide is considered as an ideal "green" oxidant for the direct oxidation of sulfides to sulfoxides due to its strength and lack of toxic by-products.[46] The rate, the chemo-, and enantioselectivity of reaction can be greatly improved by the use of catalysts such as (salen)Mn^{III} Schiff-base complexes and halogen-mediated oxidation including molecular halogens, hexafluoro-2-proponal and *N*-bromosuccinimide.[46, 50, 52-53] Still, many reported methods disclosed disadvantages like long reaction times, expensive and contaminated reagents and catalysts, and poor selectivities.

Recently, extensive studies on the epoxidation, hydroxylation and sulfoxidation catalyzed by transition metal complexes using clean and safe oxygen source such as hydrogen peroxide and molecular oxygen are being given considerable attention in view of understanding the biological processes.[53-54] *trans*-Dioxoruthenium(VI) porphyrins catalyzed hydrocarbon oxidation reactions are well established in the scientific literature in the early 80s by Groves and co-workers.[4, 55] However, the catalytic methods on sulfoxidation reactions by the well-characterized ruthenium porphyrins rarely provide the ideal combination of selectivity, fast reaction kinetics, and high product yields. The search for the efficient and selective catalytic oxidation reactions for the sulfoxide preparation has continued to be the interest of chemical research.

2. EXPERIMENTAL SECTION

2.1 Materials

All the organic solvents for synthesis and purification, including acetone, acetonitrile, chloroform, dichloromethane, ethanol, ethyl acetate, hexane, methanol and *N*, *N*-dimethylformamide (DMF), were of analytical grade and used as received without further purification. All reactive substrates for kinetic and catalytic studies were the best available purity from Aldrich Chemical Co., including thioanisole, 4-methoxy thioanisole, methyl *p*-tolyl sulfide, 4-fluorothioanisole, 4-chlorothioanisole, 4-bromothioanisole, diallylsulfide, allyl phenyl sulfide, ethyl vinyl sulfide, phenyl vinyl sulfide, 2, 2'-thiodiethanol, 4-(methylthio)benzyl alcohol, *cis*-cyclooctene, diphenylmethane and cyclohexene. The pyrrole was obtained from Aldrich Chemical Co. and freshly distilled before use. 1,2,4-Trichlorobenzene and diphenylmethane used as solvent and internal standard, mesitaldehyde, 2,3,4,5,6-pentafluorobenzaldehyde, boron trifluoride diethyl etherate ($BF_3 \cdot OEt_2$), 2,3-dichloro-5,6-dicyano-*p*-benzequinone (DDQ), triethylamine, iodobenze diacetate [$PhI(OAc)_2$], iodosylbenzene (PhIO), 2,6-dichloropyridine, triruthenium dodecacarbonyl, decahydronaphthalene (decalin), *meta*-chloroperoxybenzoic acid (*m*-CPBA), 5,10,15,20-tetrakis(pentafluorophenyl)porphyrin (H_2TPFPP), anthracene, chloroform-*d*, acetonitrile-d_3, methanol-d_4, benzene-d_6, hydrogen peroxide, and *tert*-butly hydroperoxide (TBHP), were purchased from Aldrich Chemical Co. and also used as received.

2.2 Methods

2.2.1 Physical measurements

UV-vis spectra were recorded on an Agilent 8453 diode array spectrophotometer (Figure 5). IR spectra were obtained on a Bio-Rad FT-IR spectrometer. ^{1}H-NMR was performed on a JEOL ECA-500 MHz spectrometer at 298K with tetramethylsilane (TMS) as internal standard. Gas Chromatograph analyses were conducted on an Agilent GC6890/MS5973 equipped with a flame ionization detector (FID) using a DB-5 capillary column. The above GC/MS system is also coupled with an auto simple injector. Reactions of $Ru^{II}(Por)(CO)$ and $Fe^{III}(Cor)\cdot(OEt_2)_2$ with excess of $PhI(OAc)_2$ were conducted in a chloroform and methanol solutions, respectively, at 23 ± 2 ^{o}C.

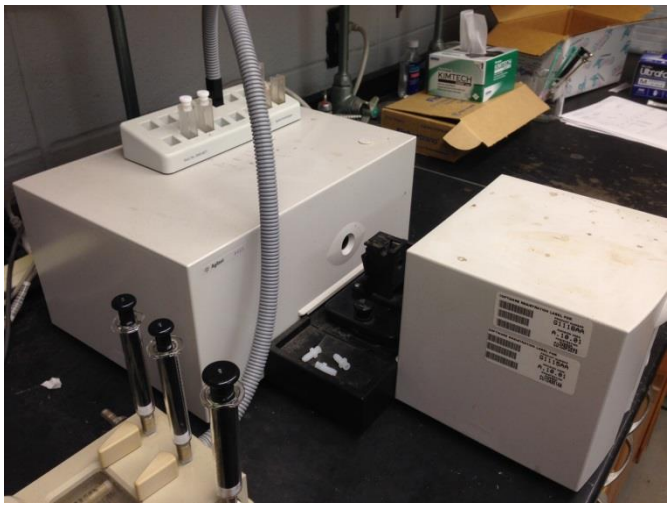

Figure 5. Agilent 8453 diode array spectrophotometer.

2.2.2 Reagent purification

The commercially available pyrrole was purified by distillation. Pyrrole (ca. 25 mL) was added into 50 mL round-bottom flask which contained a magnetic spin vane and

a distillation apparatus. The solution was heated and conducted with a short-path apparatus from ChemGlass. Since reaching the boiling point of the pyrrole at 130 ^{o}C, all the distillate was collected and below that temperature was abandoned. The freshly distilled colorless pyrrole was directly used for the synthesis of the free porphyrin and corrole ligands.

2.2.3 Photocatalytic sulfoxidations

In general, a Rayonet photoreactor (RPR-100) with a wavelength range of 400-500 nm (λ_{max}= 420 nm) from 300 W mercury visible lamps (RPR-4190×12) was used for the photocatalytic reactions (Figure 6). The photochemical reactions typically consisted of approximate 0.5-1 μmol of Ru^{II}(Por)(CO) in 2 mL of chloroform solution containing 0.5 mmol of organic substrates, 1.5 equivalent of $PhI(OAc)_2$ oxygen source (0.75 mmol). The reaction solution was then irradiated at 25 ± 2 ^{o}C until the reaction was complete. Aliquots of the reaction solution were analyzed by ^{1}H-NMR or GC/MS spectrometer to determine the product yields with an internal standard (diphenylmethane). All reactions were run at least in two times, and the data reported in the results sections represent the average of these reactions. Monitoring reaction by UV-vis spectroscopy (Agilent 8453) before and after reactions showed that no significant degradation of all catalysts was found after 24 h photolysis.

Figure 6. Rayonet photoreactor (RPR-100) with 300 W mercury visible lamps (λ_{max}= 420 nm, RPR-4190×12).

2.2.4 Competitive catalytic oxidations

A reaction containing equal amounts of two substrates, e.g. thioanisole (0.5 mmol) and substituted thioanisole (0.5 mmol), ruthenium(II) porphyrin catalyst (1 μmol) and an internal standard of diphenylmethane (0.1 mmol) was prepared in 5 mL of $CHCl_3$ solution. The internal standard was shown to be stable to the oxidation conditions in control reactions. $PhI(OAc)_2$ (0.4 mmol) as limiting reagent was added, and the mixture was irradiated under visible lights at ambient temperature (25 ± 2 ^oC) until the reaction was complete. Relative rate ratios for oxidations were determined based on the amounts of products (sulfoxides) by ^{1}H-NMR or GC (FID, DB-5). All reactions were run at least in 2-3 times, and the data reported later represent the average of these reactions.

2.2.5 Photocatalytic aerobic oxidations

A Rayonet photoreactor (RPR-100) with a wavelength range of 400-500 nm (λ_{max}= 420 nm) from 300 W mercury lamps (RPR-4190×12) was used for the photocatalytic reactions. The photochemical reactions typically consisted of 1.0 mg of $[Fe^{IV}(TPFC)]_2O$ in 5 mL of acetonitrile containing over 4 mmol of organic substrates. In most cases, 5 ~ 10 mg of anthracene was added to enhance the catalytic activity. Dry and pure oxygen gas was bubbled through the solution as it was irradiated. Aliquots of the reaction solution were analyzed by GC/MS spectrometer to determine the formed products and yields with 1,2,4-trichlorobenzene as an internal standard. Monitoring reaction by UV-vis spectroscopy indicated that no significant degradation of catalyst was found after 24 h photolysis. Turnover number (TON) is calculated based on the following definition:

TON = moles of oxidized products / moles of catalyst used

2.2.6 Catalytic sulfoxidations by metallocorroles

The catalytic reactions typically consisted of approximate 0.5-1 μmol of $Fe^{III}(Cor)\cdot(OEt_2)_2$ in 2 mL of methanol solution containing 0.5 mmol of organic substrates, 1.5 equivalent of $PhI(OAc)_2$ oxygen source (0.75 mmol). The reaction solution was stirred at 25 ± 2 ^oC until the reaction was complete. Aliquots of the reaction solution were analyzed by ^1H-NMR or GC/MS spectrometer to determine the product yields with an internal standard (diphenylmethane). All reactions were run at least in two times, and the data reported represent the average of these reactions.

2.3 Synthesis and spectroscopic characterization

2.3.1 *meso*-Tetramesitylporphyrin [H_2TMP] (**1a**)

The sterically encumbered free porphyrin ligand was prepared based on the well-known method described by Lindsey and co-workers,[56] as shown in Scheme 6. l-L round-bottomed flask fitted with reflux condenser was charged with freshly distilled pyrrole (347 μL, 5 mmol), mesitaldhyde (736 μL, 5 mmol) and chloroform (500 mL). Ethyl alcohol (3.47 mL, 0.5% v/v) was added as co-catalyst. The solution was purged with Argon for 5 min. Boron trifluoride diethyl etherate ($BF_3 \cdot OEt_2$) (660 μL, 1.65 mmol) was added in a dropwise manner, and the reaction mixture was stirred for 1.5 h at room temperature. The co-catalyst of $BF_3 \cdot OEt_2$ and ethanol generates the formation of Bronsted acid (BF_3-ROH, R= ethyl group). This Bronsted acid catalyzes the pyrrole-aldehyde condensation to form porphyrinogen.

The reaction was monitored by UV-vis spectroscopy to confirm porphyrinogen had been formed during the room temperature reaction and followed by one-electron oxidation with 2,3-dichloro-5,6-dicyano-*p*-benzequinone (DDQ) (957 mg), which was added and the reaction mixture was then gently refluxed for 1 h. After the solution was cooled to room temperature, triethylamine (920 μL, 6.6 mmol) was added to neutralize the mixture, and the solution was evaporated to dryness. The solid crude product was washed by large excess of methanol under vacuum until the filtrate was clear. The typical impurities such as poly-pyrromethanes and quinine components are highly soluble in the methanol and can be easily removed. The further purification was performed by column chromatography (silica gel). After placing the product into the wet column,

dichloromethane was used to elute the desired product. The *meso*-tetramesitylporphyrin (H_2TMP, **1a**) was obtained as purple solid after rotary evaporation and characterized by UV-vis (Figure 7) and ^{1}H–NMR (Figure 8), matching literature reported values.[56]

[H_2TMP] (**1a**) Yield = 25.1%. ^{1}H-NMR (500 MHz, $CDCl_3$): δ, ppm: -2.50 (s, 2H, NH), 1.81 (s, 24H, *o*-CH_3), 2.62 (s, 12H, *p*-CH_3), 7.25 (s, 8H, *m*-ArH), 8.61 (s, 8H, *β*-pyrrole). UV-vis (CH_2Cl_2) λ_{max}/nm: 418 (Soret), 441, 513, 546, 594, 645.

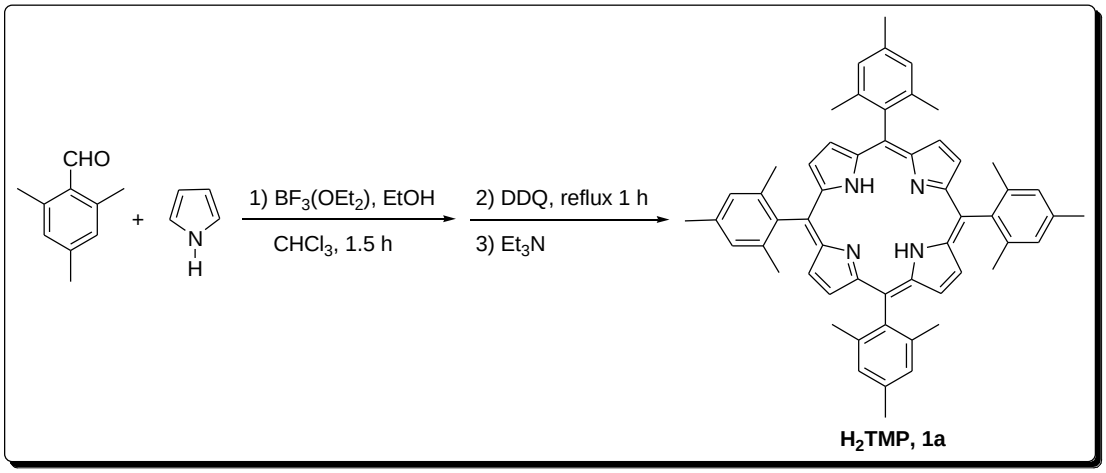

Scheme 6. Two-step and one-pot synthesis of H_2TMP (**1a**).

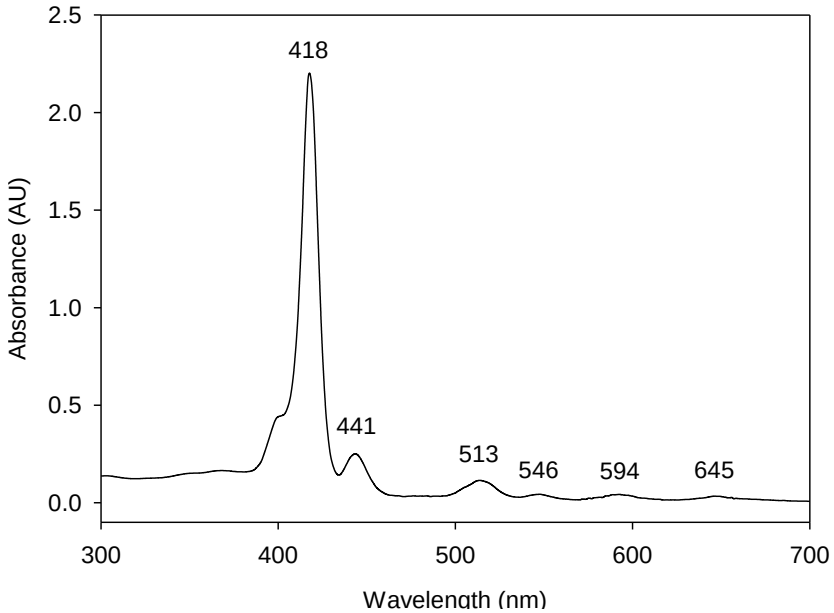

Figure 7. The UV-vis spectrum of H_2TMP (**1a**) in CH_2Cl_2.

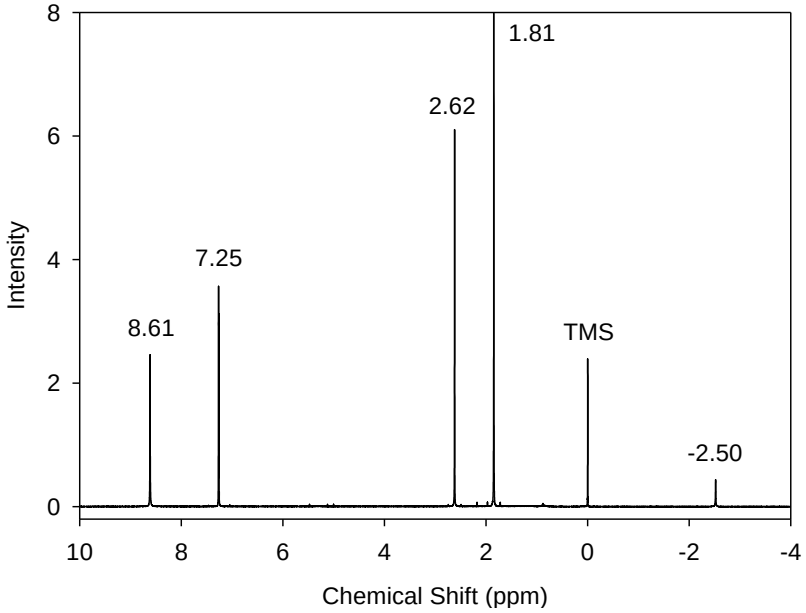

Figure 8. The ^{1}H-NMR spectrum of H_2TMP (**1a**) in $CDCl_3$.

2.3.2 Ruthenium(II) carbonyl porphyrins [Ru^{II}(Por)(CO)] (**2**)

The ruthenium(II) carbonyl porphyrins were synthesized according to the method described by Che and co-workers,[55] as shown in Scheme 7.[18] Free porphyrin ligand of **1a** or 5,10,15,20-tetrakis(pentafluorophenyl)porphyrin (H_2TPFPP) (**1b**) (100 mg) was dissolved in 50 mL of 1,2,4-trichlorobenzene in a round bottom-flask and the reaction was gently heated with stirring to ca. 100 ^{o}C. Excess of triruthenium dodecacarbonyl [$Ru_3(CO)_{12}$] (150 mg) was added and the solution was refluxed at 220 ^{o}C for 1 h. A long refluxing time (12 h) was required for the preparation of the electron-efficient ruthenium(II) carbonyl tetrapentafluoroporphyrin Ru^{II}(TPFPP)(CO) (**2b**) due to more electron-withdrawing nature of the free ligands (**1b**).

UV-vis spectroscopy was used to monitor the Soret band of the metal complex product based on literature values. The mixture was cooled to room temperature, and product was separated and purified by column chromatography (basic Al_2O_3). The column was loaded by crude product mixture followed by a large excess amount of hexane to remove 1,2,4-trichlorobenzene. Hexane dichloromethane (1:1, v/v) was used to elute the remaining free ligand. Dichloromethane was then utilized to elute the desired product. The brick-red solid was obtained after removing the solvent via rotary evaporation. The metalloporphyrin Ru^{II}(TMP)(CO) (**2a**) and Ru^{II}(TPFPP)(CO) (**2b**) were characterized by UV-vis (Figure 9 and 11) and ^{1}H-NMR (Figure 10 and 12), matching literature reported values.[57]

[Ru^{II}(TMP)(CO)] (**2a**). Yield = 95%. ^{1}H-NMR (500 MHz, $CDCl_3$): δ, ppm: 1.84 (s, 24H, *o*-CH3), 2.60 (s, 12H, *p*-CH3), 7.24 (s, 8H, *m*-ArH), 8.45 (s, 8H, *β*-pyrrole). UV-vis (CH_2Cl_2) λ_{max}/nm: 412 (Soret), 530.

[Ru^{II}(TPFPP)(CO)] (**2b**) Yield = 85%. ^{1}H-NMR (500MHz, $CDCl_3$): δ, ppm: 8.71 (s, 8H, *β*-pyrrole). UV-vis (CH_2Cl_2) λ_{max}/nm: 402 (Soret), 524.

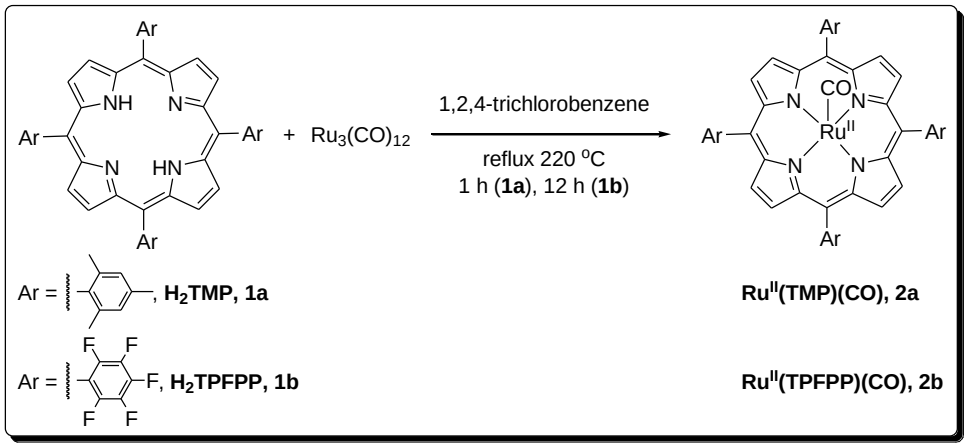

Scheme 7. Synthesis of Ru^{II}(Por)(CO) (**2**).

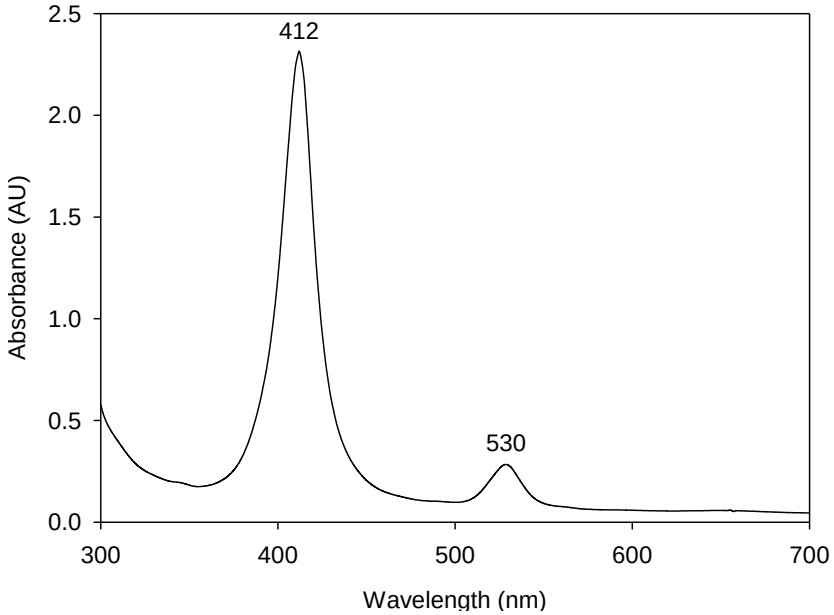

Figure 9. The UV-vis spectrum of Ru^{II}(TMP)(CO) (**2a**) in CH_2Cl_2.

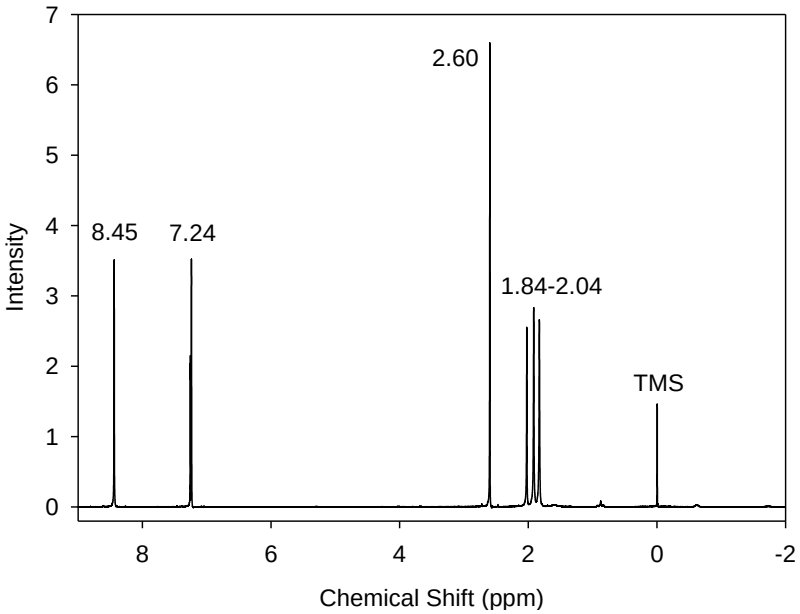

Figure 10. The ^{1}H-NMR spectrum of Ru^{II}(TMP)(CO) (**2a**) in $CDCl_3$.

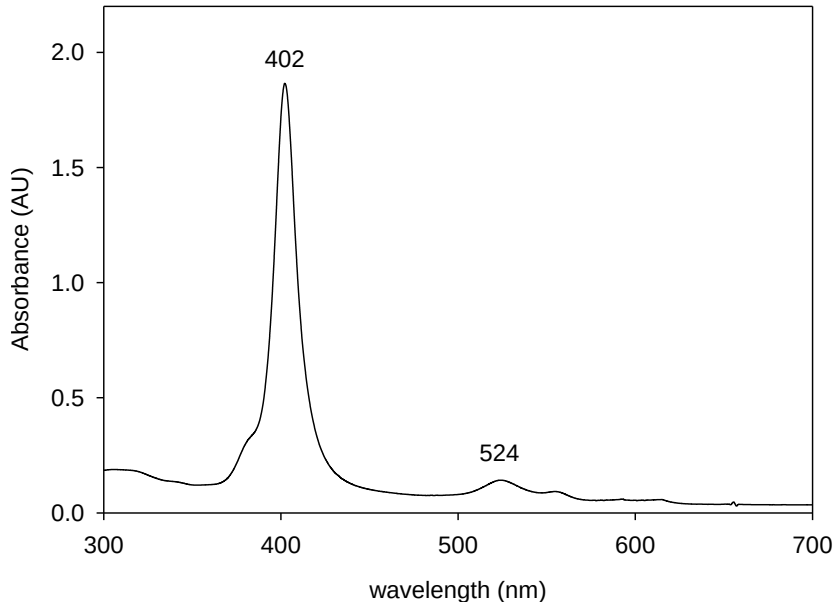

Figure 11. The UV-vis spectrum of Ru^{II}(TPFPP)(CO) (**2b**) in CH_2Cl_2.

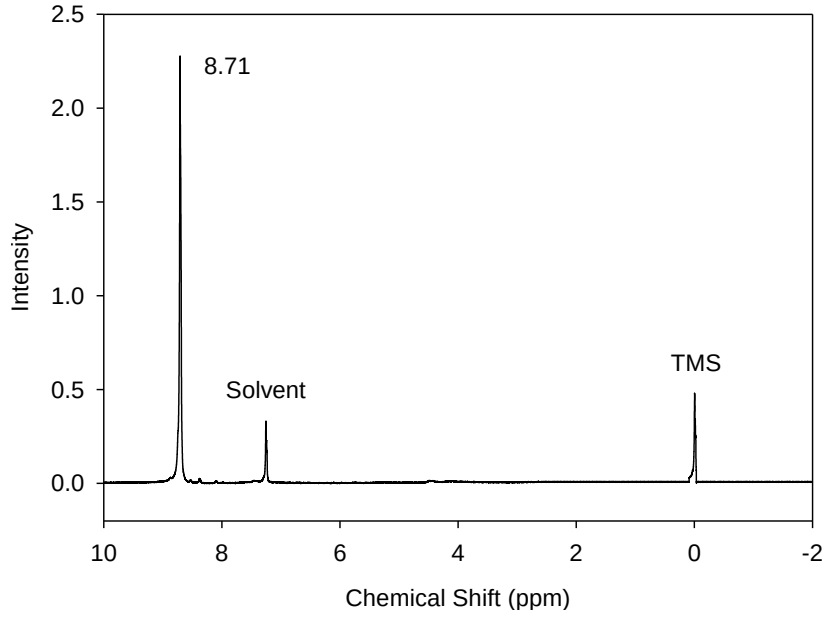

Figure 12. The ^{1}H-NMR spectrum of Ru^{II}(TPFPP)(CO) (**2b**) in $CDCl_3$.

2.3.3 5,10,15-Triphenylcorrole [H_3TPC] (**3a**)

The corrole free ligand was prepared according to the method described by Koszarna and Gryko,[30] as shown in Scheme 8. Distilled pyrrole (697 μL, 10 mmol) and benzealdehyde (509 μL, 5 mmol) were dissolved in MeOH (200 mL) in a 1-L round-bottom flask. Distilled water (200 mL) was added into the solution. After the reaction mixture was purged with argon, concentrated HCl_{aq} (36%, 4.25 mL) as the acid catalyst was added into the reaction mixture in a dropwise manner. The reaction was stirred at room temperature for 3 hr. The reaction was monitored by UV-vis spectroscopy.

The reaction mixture was then extracted with $CHCl_3$ for three times. The organic layer was washed with deionized water (3× 100 mL) to eliminate the residual HCl_{aq}. The mixture was dried over Na_2SO_4, filtered and then diluted to 300 mL of $CHCl_3$. *p*-Chloranil (1.23 g, 5 mmol) as oxidant was added, and the mixture was gently refluxed for 1 h. UV-vis was used to monitor the reaction throughout this oxidation process. The final product was separated and purified on a wet column (silica gel) and eluted with CH_2Cl_2. The dark-green solid was obtained when the solvent was removed via rotary evaporation. The desired product H_3TPC (**3a**) was characterized by UV-vis (Figure 13) and 1H-NMR (Figure 14), consistent with the literature reported.[30]

[H_3TPC] (**3a**) Yield =17.2%. ^{1}H-NMR (500 MHz, $CDCl_3$): δ, ppm: -2.90 (s, 3H, NH), 7.73-7.83 (m, 9H), 8.17 (d, 2H), 8.38 (d, 4H), 8.55 (d, 2H), 8.60 (d, 2H), 8.87 (d, 2H), 8.95 (d, 2H). UV-vis (CH_2Cl_2) λ_{max}/nm: 415 (Soret), 567, 615, 648.

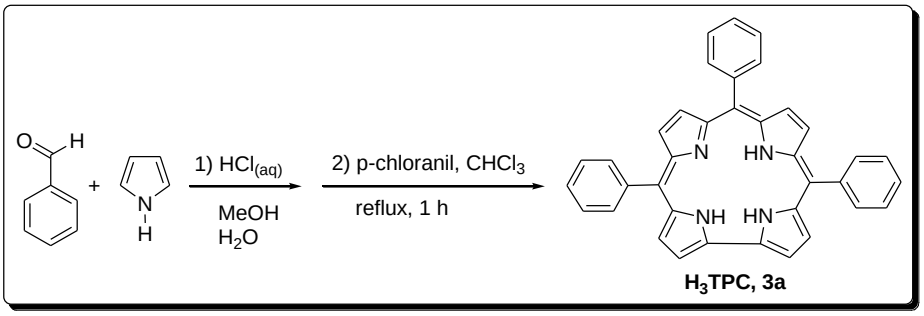

Scheme 8. Synthesis of H_3TPC (**3a**).

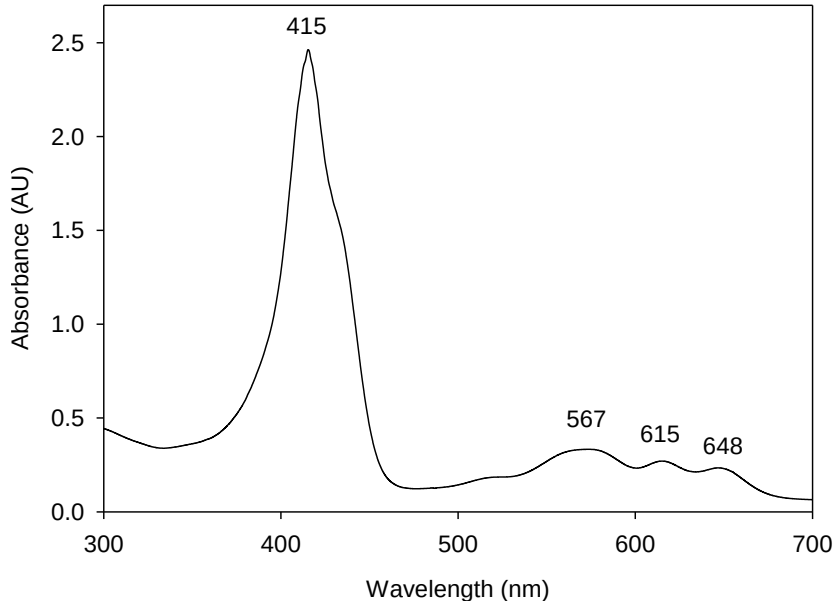

Figure 13. The UV-vis spectrum of H_3TPC (**3a**) in CH_2Cl_2.

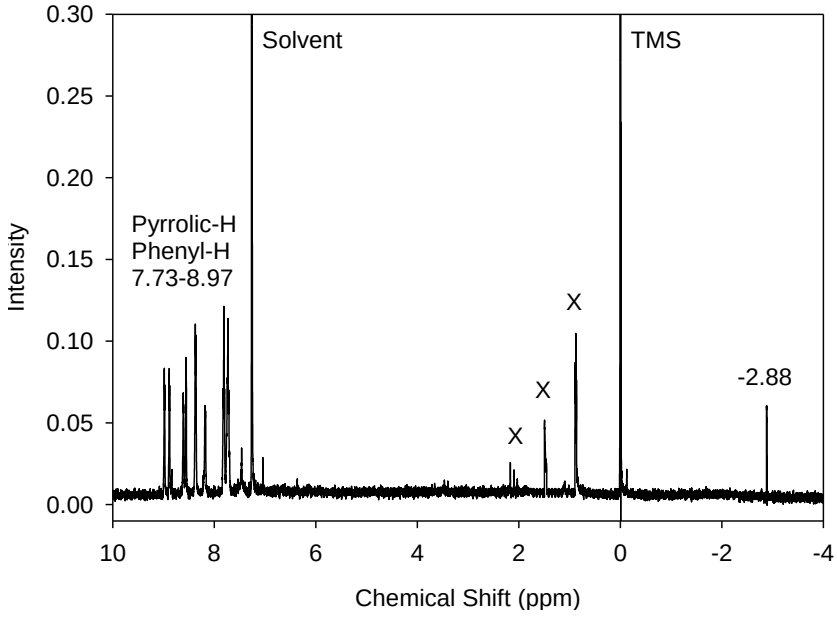

Figure 14. The ^{1}H-NMR spectrum of H_3TPC (**3a**) in $CDCl_3$.

2.3.4 5,10,15-Tri(pentafluorophenyl)corrole [H_3TPFC] (**3b**)

Solvent-free condensation of pyrrole and pentafluorobenzaldehyde is an efficient synthetic pathway to prepare corroles based on Zeev Gross and co-workers,[32] as shown in Scheme 9. Pentafluorobenzaldehyde (2.94 g, 15 mmol) and pyrrole (1.04 mL, 15 mmol) were dissolved in CH_2Cl_2 (5~10 mL). The mixture was then added to a 20 mL beaker containing basic alumina oxide (3 g) as a solid support and then the mixture was heated with stirring in an open vessel to 60 ^{o}C (inner temperature). Once the CH_2Cl_2 had been evaporated, the reaction was maintained at 60 ^{o}C for 4 hours. The mixture became dark brown and black. CH_2Cl_2 (50mL) was then added to dissolve tarry product and the solution was filtered through vacuum. The filtrate was stirred with by DDQ (1.7 g, 7.5 mmol) for 1 h. The reaction progress was checked by TLC (dichloromethane/hexanes = 1:1), and a purple band with strong fluorescence under long-wave UV light could be seen.

The isolation and purification of final product was performed on a long column (basic Al_2O_3) with hexane / CH_2Cl_2 (3:1, v/v) as eluent. The second column might be necessary as needed. The desired product H_3TPFC (**3b**) was characterized by UV-vis (Figure 15) and ^{1}H-NMR (Figure 16), matching the literature reported.[58]

[H_3TPFC] (**3b**) Yield = 7%. ^{1}H-NMR (500 MHz, $CDCl_3$): δ, ppm: -2.25 (s, 3H), 8.57 (d, 4H), 8.75 (d, 2H), 9.10 (d, 2H). UV-vis (CH_2Cl_2) λ_{max}/nm: 408 (Soret), 560, 602.

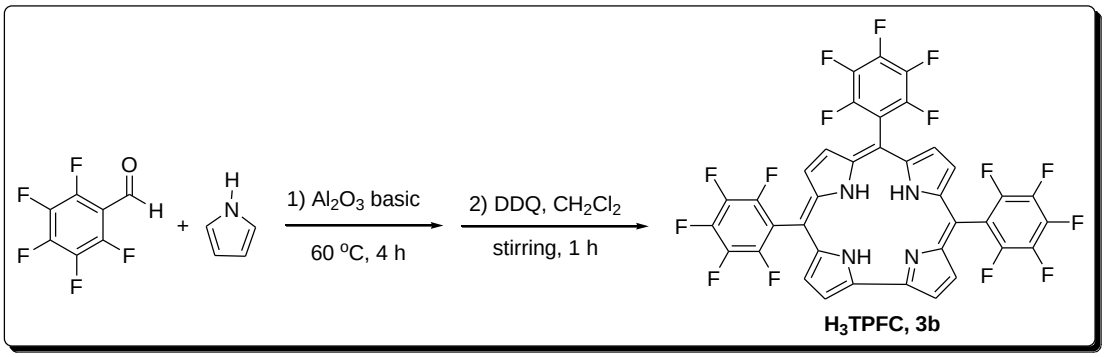

Scheme 9. Synthesis of H_3TPFC (**3b**).

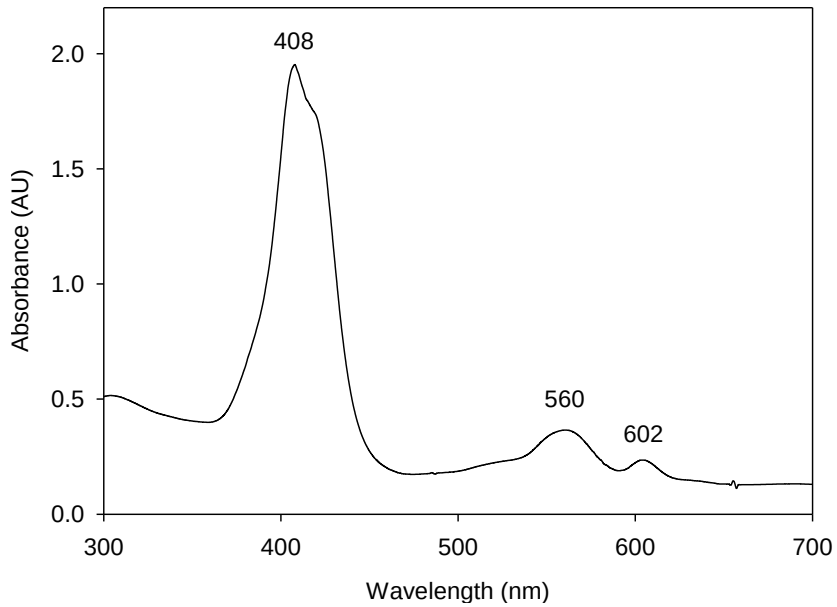

Figure 15. The UV-vis spectrum of H_3TPFC (**3b**) in CH_2Cl_2.

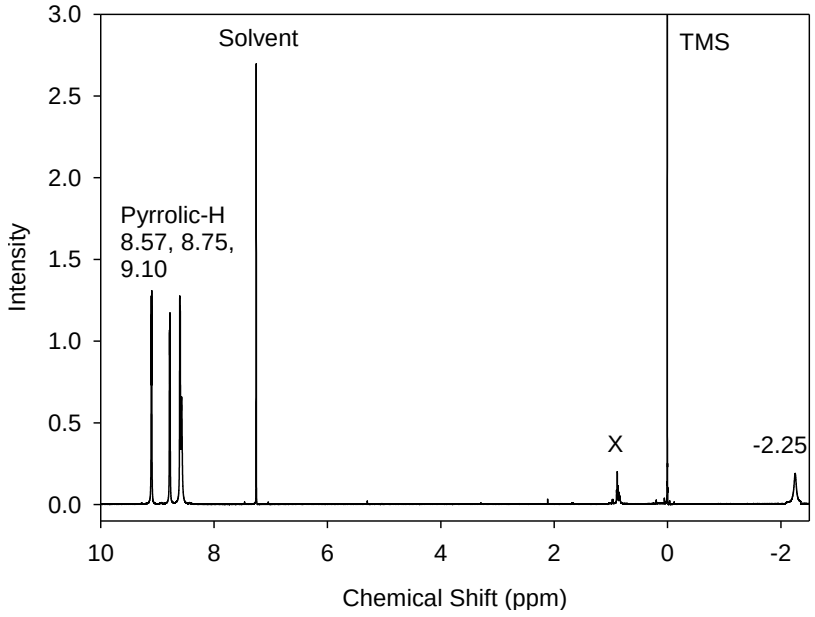

Figure 16. The ^{1}H-NMR spectrum of H_3TPFC (**3b**) in $CDCl_3$.

2.3.5 5,10,15-Tris(4-nitrophenyl)corrole [H_3TNPC] (**3c**)

According to Paolesse and his co-workers' method,[59] as shown in Scheme 10, acetic acid (250 mL) were placed into a 500 mL round-bottom flask with fitted reflux condenser. 4-nitrobenzaldehyde (3.05 g, 20.2 mmol) and distilled pyrrole (4.2 mL, 60.5 mmol) were added and dissolved in the flask. The reaction mixture was mildly refluxed under stirring for 3 hr. The reaction mixture was cooled to room temperature. The saturated NaCl solution was added to the filtrate and the solution was kept in ice bath to accelerate precipitation. The resulting precipitate was filtered off and washed by saturated NaCl solution until the filtrate was clear. The crude solid was dissolved in CH_2Cl_2 and dried over Na_2SO_4. The final product was chromatographed through short column of silica gel eluting with CH_2Cl_2. The fractions were collected and evaporated to dryness.

The desired product of H_3TNPC (**3c**) was characterized by UV-vis (Figure 17) and ^{1}H-NMR (Figure 18), matching literature reported.[59]

[H_3TNPC] (**3c**) Yield = 10.1%. ^{1}H-NMR (500 MHz, $CDCl_3$) δ: -2.83 (s, 3H), 8.42 (t, 3H), 8.52 (d, 4H), 8.57 (d, 2H), 8.65 (m, 2H), 8.73 (d, 4H), 8.82 (s, 1H), 8.90 (d, 2H), 9.12 (d, 2H). UV-vis (CH_2Cl_2) λ_{max}/nm: 425 (Soret), 594.

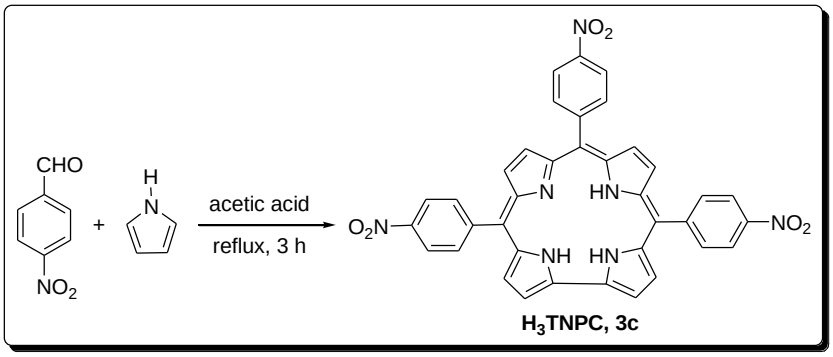

Scheme 10. Synthesis of H_3TNPC (**3c**).

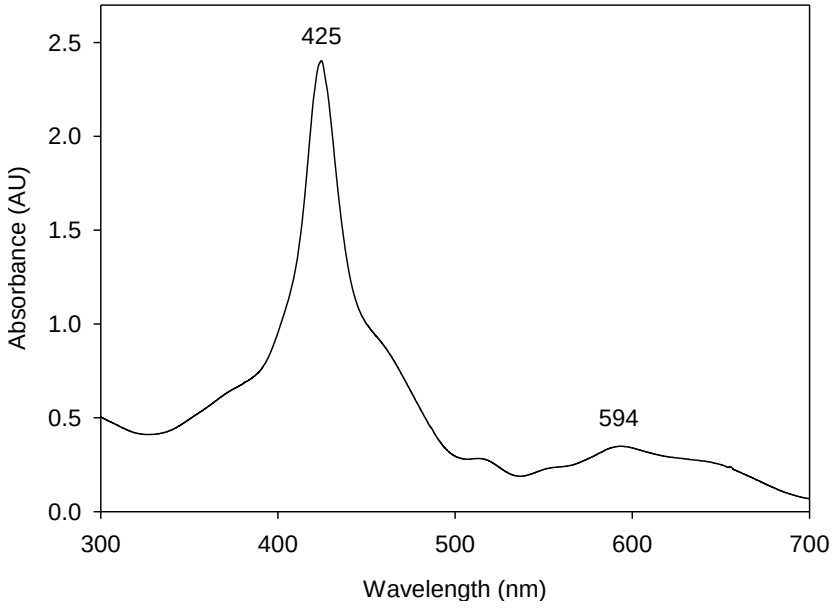

Figure 17. The UV-vis spectrum of H_3TNPC (**3c**) in CH_2Cl_2.

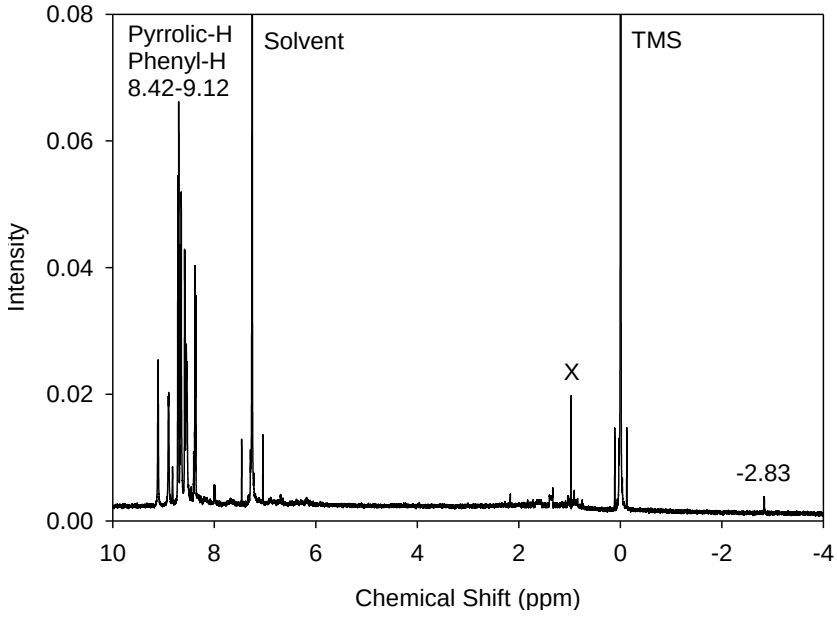

Figure 18. The ^{1}H-NMR spectrum of H_3TNPC (**3c**) in $CDCl_3$.

2.3.6 Iron(III) corroles [Fe^{III}(Cor)·$(OEt_2)_2$] (**4**)

Corrole-iron(III) complexes were obtained by metalation of free corrole ligand [H_3TPC (**3a**), H_3TPFC (**3b**), or H_3TNPC (**3c**)] in hot DMF with $FeCl_2$ as the metal source (Scheme 11). According to the procedure described by Simkhovich et al.[60] a solution of free corrole ligands (**3a-c**) (50 mg, 68 mmol) was dissolved in DMF (30 mL) in a two-neck 100-mL round-bottom flask fitted with reflux condenser. The solution was purged with argon and heated mildly to be warm. Large excess amount of iron(II) chloride ($Fe^{II}Cl_2$) (127 mg, 680 mmol) was added. The mixture was heated under gentle stirring for 1 hr. UV-vis spectroscopy was used to monitor the reaction process.

The reaction mixture was cooled to room temperature. High boiling point solvent DMF was removed by vacuum distillation. Crude and solid product was collected and dissolved with diethyl ether, then followed by a column chromatography on silica gel

(diethyl ether). Isolation of the desired metallocorrole complexes **4 (a, b, c)** were characterized by UV-vis (Figure 19, 21 and 23) and ^{1}H-NMR (Figure 20, 22 and 24), consistent with the pattern of paramagnetic compound.[61]

[Fe^{III}(TPC)·$(OEt_2)_2$] (**4a**) Yield = 33.4%. ^{1}H-NMR (500 MHz, C_6D_6): δ, ppm: 25.26, 24.05, 23.18, 19.70, 17.34, -2.61, -3.73, -5.85, -7.00, -41.23. UV-vis (diethyl ether) λ_{max}/nm: 362, 408, 635.

[Fe^{III}(TPFC)·$(OEt_2)_2$] (**4b**) Yield = 85%. ^{1}H-NMR (500 MHz, C_6D_6): δ, ppm: 19.71 (s, 2H), 13.37 (s, 2H), -60.03 (s, 2H), -126.05 (s, 2H). UV-vis (diethyl ether) λ_{max}/nm: 404, 546.

[Fe^{III}(TNPC)·$(OEt_2)_2$] (**4c**) Yield= 70.9%. ^{1}H-NMR (500 MHz, C_6D_6): δ, ppm: 23.64, 22.55, 21.61, -1.32, -2.36, -5.89, -7.55, -38.98. UV-vis (diethyl ether) λ_{max}/nm: 362, 416, 579.

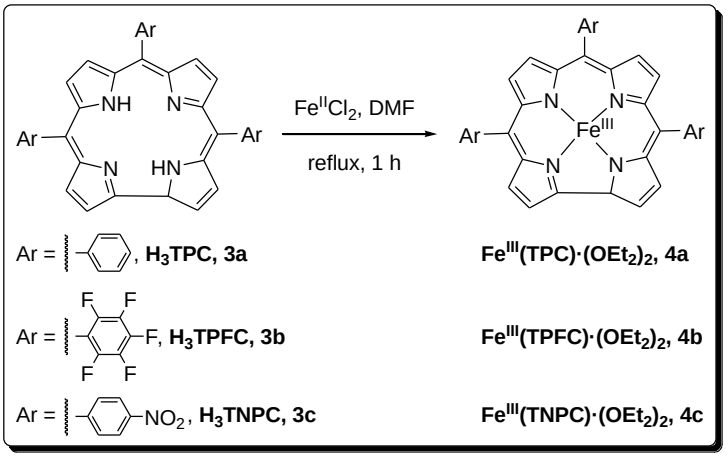

Scheme 11. Synthesis of Fe^{III}(Cor)·$(OEt_2)_2$ (**4**).

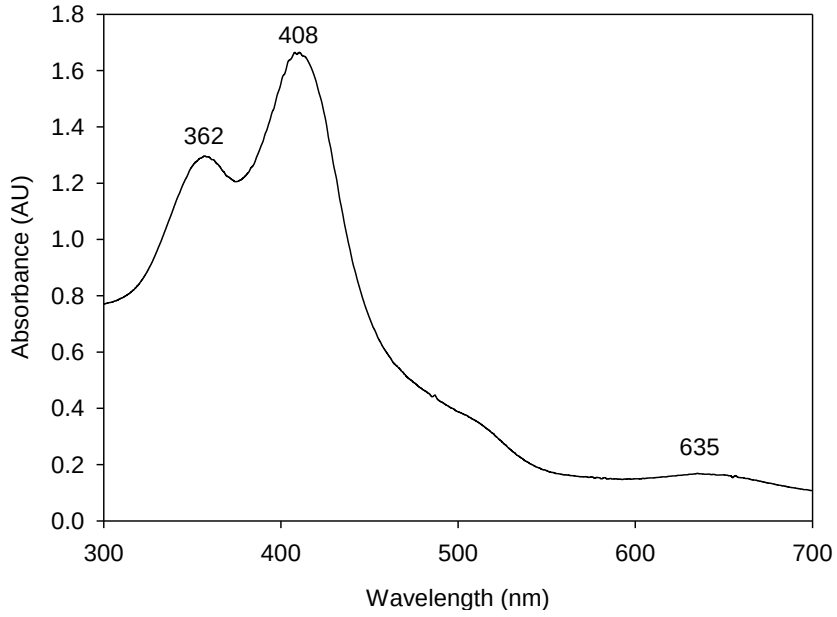

Figure 19. The UV-vis spectrum of $Fe^{III}(TPC)\cdot(OEt_2)_2$ (**4a**) in diethyl ether.

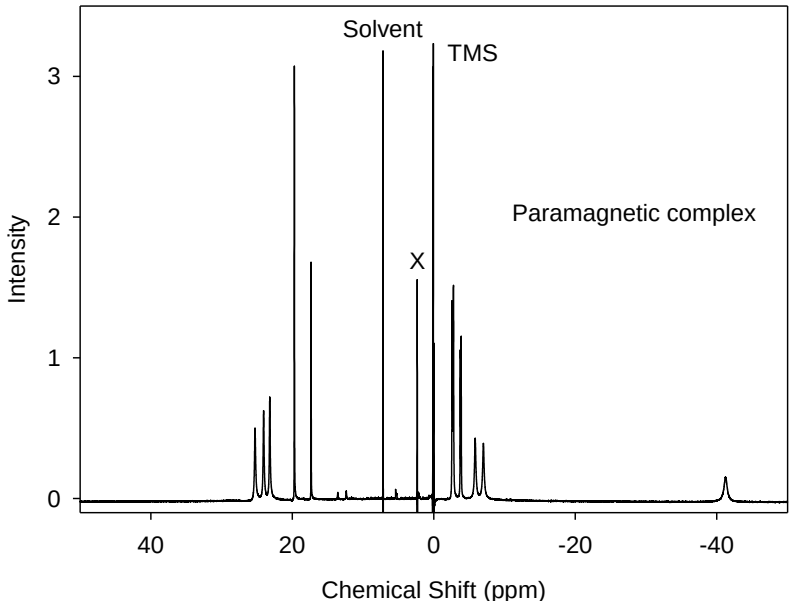

Figure 20. The ^{1}H-NMR spectrum of $Fe^{III}(TPC)\cdot(OEt_2)_2$ (**4a**) in C_6D_6.

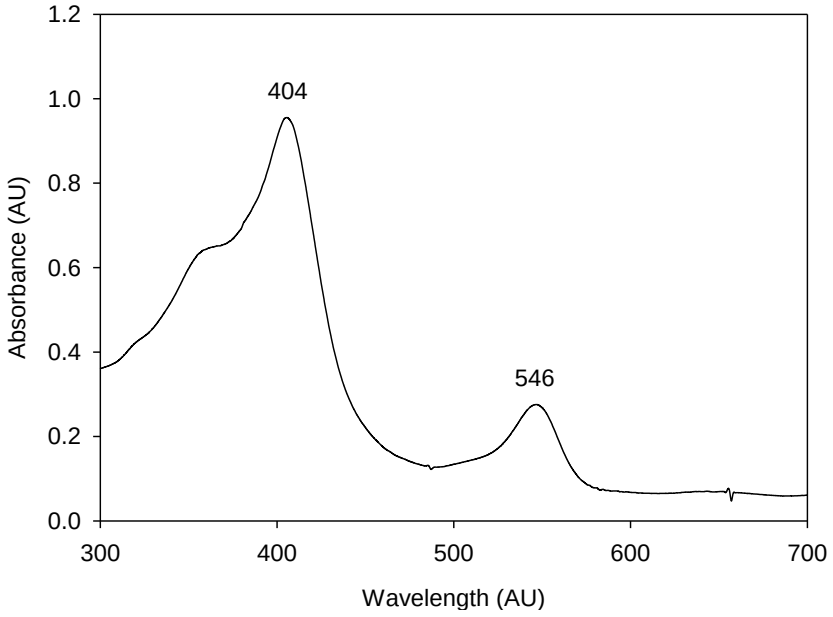

Figure 21. The UV-vis spectrum of $Fe^{III}(TPFC)\cdot(OEt_2)_2$ (**4b**) in diethyl ether.

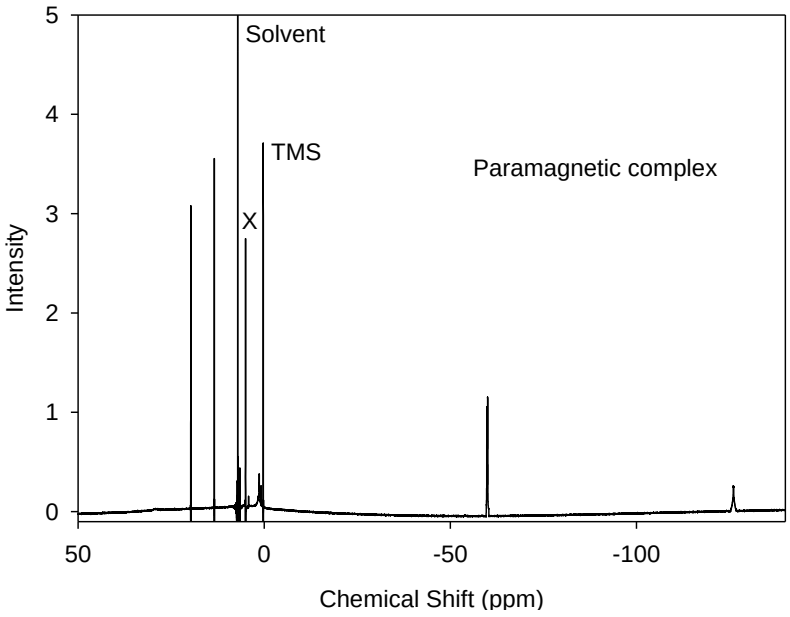

Figure 22. The ^{1}H-NMR spectrum of $Fe^{III}(TPFC)\cdot(OEt_2)_2$ (**4b**) in C_6D_6.

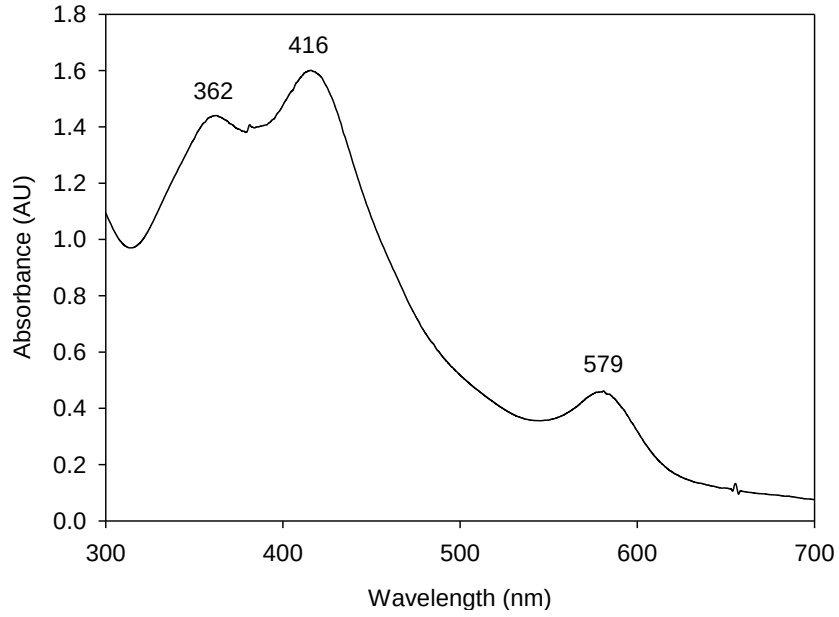

Figure 23. The UV-vis spectrum of $Fe^{III}(TNPC)\cdot(OEt_2)_2$ (**4c**) in diethyl ether.

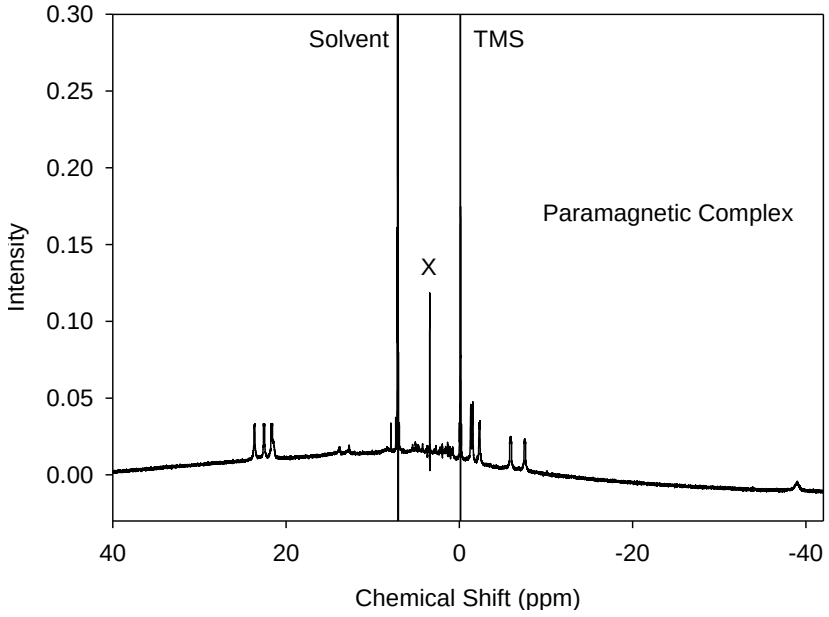

Figure 24. The ^{1}H-NMR spectrum of $Fe^{III}(TNPC)\cdot(OEt_2)_2$ (**4c**) in C_6D_6.

2.3.7 Diiron(IV) μ-oxo biscorrole complex $[Fe^{IV}(Cor)]_2O$ (**5**)

Diiron(IV) μ-oxo biscorrole (**5**), formulated as $[Fe^{IV}(Cor)]_2O$, was readily prepared by aerobic oxidation of monomeric precursors $Fe^{III}(Cor)\cdot(OEt_2)_2$ (**4**) in a solution of oxygen-saturated acetonitrile and *n*-heptane (Scheme 12), according to the procedure described by Zeev Gross and co-workers.[61] However, only the diiron(IV) μ-oxo-bis(5,10,15-tripentafluorocorrole) complex **5b** was obtained and characterized by UV-vis (Figure 25 and 27) and ^{1}H-NMR (Figure 26) that matched those previously reported.[61]

It is worth mentioning that electron-withdrawing substituents such as F and NO_2 on corrole ligand are necessary for μ-oxo dimer formation and using the same procedure by reacting the iron(III) complex with a non-halogenated 5,10,15-triphenylcorrole; i.e. Fe^{III}(TPC) (**4a**) in air did not give the corresponding μ-oxo products. Presumably, the electron-withdrawing subsitutents would stabilize the iron(IV) complex in a dimeric form by reducing the electron density of metal atoms. In our recent study, we also found the marked dependence of formation of ruthenium(IV) μ-oxo bisporphyrins on the electron-withdrawing substituents on phenyl ring.[62]

$[Fe^{IV}(TPFC)]_2O$ (**5b**). ^{1}H-NMR (500 MHz, $CDCl_3$): δ, ppm: 6.44 (d, 4H), 6.50 (d, 4H), 6.79 (d, 4H), 7.07 (d, 4H). UV-vis (CH_3CN) λ_{max}/nm: 380.

$[Fe^{IV}(TPC)]_2O$ (**5c**). UV-vis (CH_3CN) λ_{max}/nm: 382.

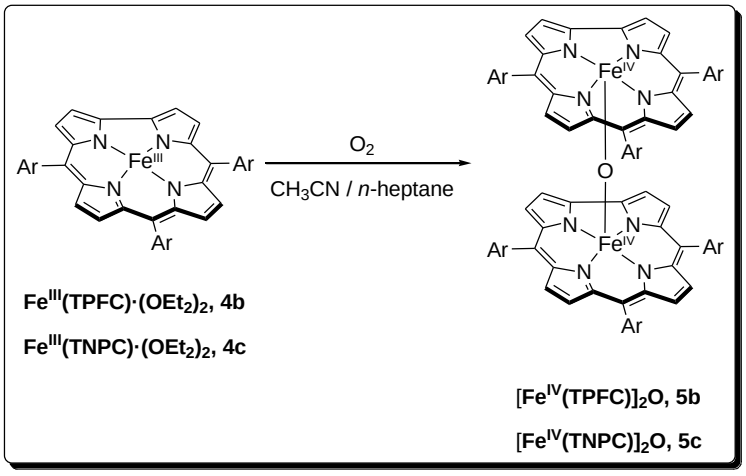

Scheme 12. Synthesis of $[Fe^{IV}(Cor)]_2O$ (**5**).

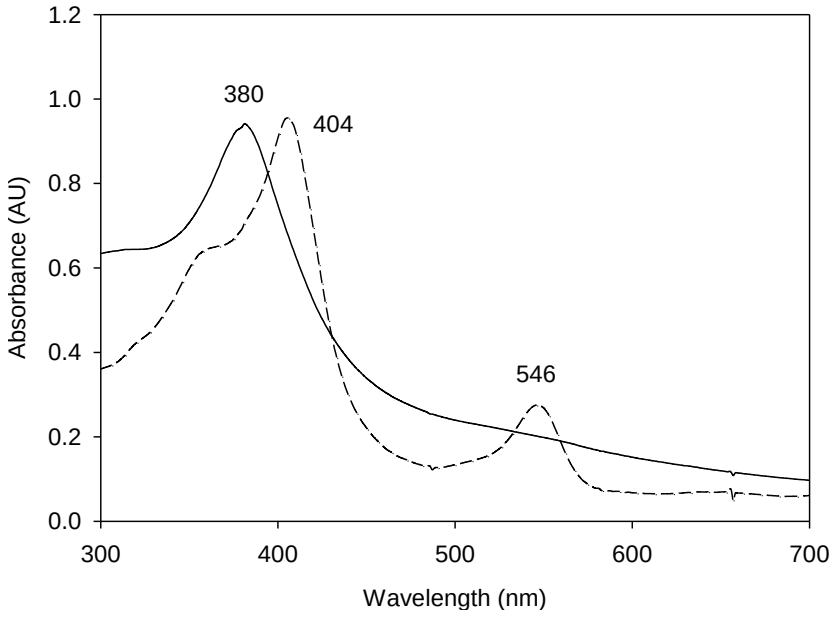

Figure 25. The UV-vis spectra of $[Fe^{IV}(TPFC)]_2O$ (**5b**) (solid line) and $Fe^{III}(TPFC)\cdot(OEt_2)_2$ (**4b**) (dash line) in CH_3CN.

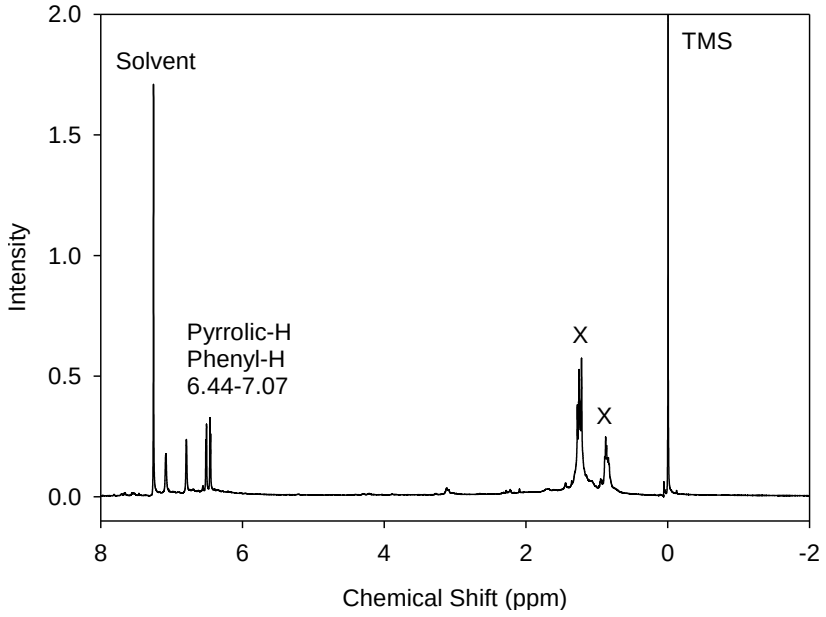

Figure 26. The ^{1}H-NMR spectrum of $[Fe^{IV}(TPFC)]_2O$ (**5b**) in $CDCl_3$.

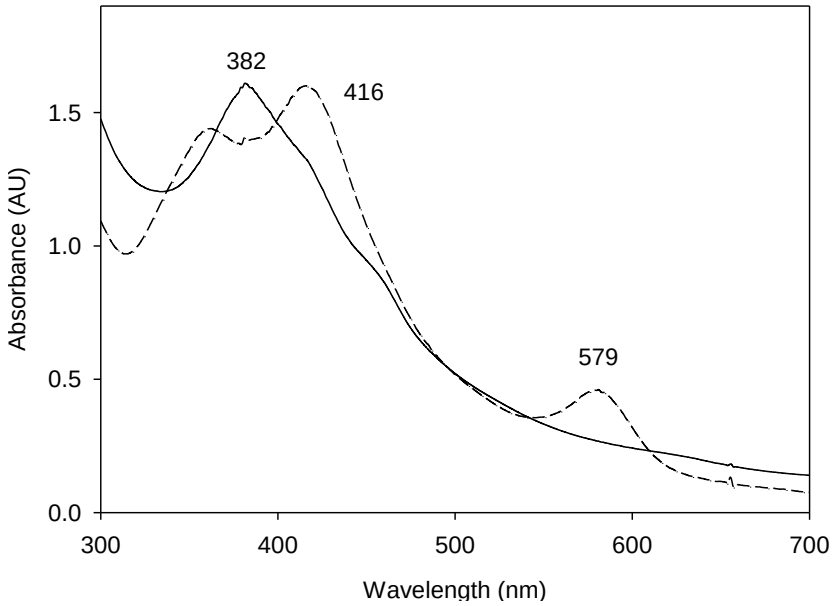

Figure 27. The UV-vis spectra of $[Fe^{IV}(TNPC)]_2O$ (**5c**) (solid line) and $Fe^{III}(TNPC)\cdot(OEt_2)_2$ (**4c**) (dash line) in CH_3CN.

3. CATALYTIC OXIDATION OF SULFIDES BY RUTHENIUM PORPHYRINS

3.1 Introduction

Ruthenium porphyrin complexes are among the most extensively studied biomimetic catalysts in view of their rich coordination and redox chemistry.[4, 63] A large number of reports on the catalytic behavior of ruthenium porphyrins have appeared in the past two decades with major focus on alkene epoxidation and activated alkane hydroxylation. The synthetic ruthenium porphyrins associated with various sacrificial oxidants such as iodosobenzene (PhIO), *tert*-butyl hydroperoxide (TBHP) and *meta*-chloroperoxybenzoic acid (*m*-CPBA) catalyze a wide variety of oxidation reactions including epoxidation, hydroxylation and oxidation of amines, sulfides, alcohols and aldehydes.[18, 57] Product turnovers of over 10,000 can be reached by recycling the catalysts several times or by performing the oxidation at low catalyst loadings.[64-65] However, only very few studies has been reported with limited success on oxidation of sulfides by these well studied ruthenium porphyrins.[66]

In this section, we aim to fully explore the potential of ruthenium porphyrins toward catalytic sulfoxidation reactions with iodobenzene diacetate [$PhI(OAc)_2$], which is commercially available and easy to handle. In contrast to the sacrificial oxidants in common use for metalloporhyrin catalyzed reactions, $PhI(OAc)_2$ does not show appreciable reactivity towards organic substrates or does not damage the porphyrin catalyst under the usual catalytic conditions. Due to the mild oxidizing ability, $PhI(OAc)_2$ has been less often employed in the matalloporphyrin-catalyzed oxidations. Collman and

Nam, Adam, and Nishiyama etc. have reported the use of $PhI(OAc)_2$ as oxidant in the metalloporphyrin catalyzed oxidation of hydrocarbons.[67-70]. In current study, we have discovered that $PhI(OAc)_2$ is an efficient oxygen source associated with ruthenium porphyrins for the selective oxidation of sulfides to sulfoxides, which is greatly promoted by visible light irradiation (Scheme 13). In all cases, quantitative conversions of sulfides and exclusive selectivities for sulfoxides were obtained. Meanwhile, we discover that a low-reactivity ruthenium(IV)-oxo porphyrin intermediate is detected by the oxidation of ruthenium(II) carbonyl precursor with $PhI(OAc)_2$, which is ascribed to the observed excellent selectivity for sulfoxide.

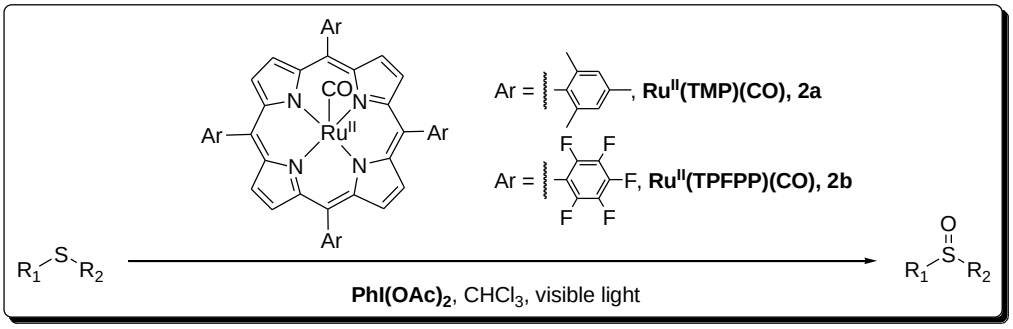

Scheme 13. Catalytic oxidation of sulfides by Ru^{II}(Por)(CO) (**2**) in the presence of $PhI(OAc)_2$ and visible light.

3.2 Results and discussions

3.2.1 Screening studies

Although the iodobenzene diacetate, $PhI(OAc)_2$, has been widely used as a mild oxidant for some time, but not been used for ruthenium porphyrin-catalyzed sulfoxidation reactions. Therefore, in this section, we have first investigated the $PhI(OAc)_2$ as oxygen source in the catalytic oxidation of thioanisole (**6a**) with different ruthenium porphyrin

catalysts to identify the most efficient systems and optimal conditions from the screening studies. In order to work under homogeneous conditions and follow the analysis via ^{1}H NMR, the reactions were performed in $CDCl_3$ at room temperature using a 0.2 mol% catalyst loading and a 1:1.5 ration of thioanisole and $PhI(OAc)_2$. Our results collected in Figure 28 and Table 1 show the Ru^{II}(TMP)(CO) (**2a**) catalyzed the oxidation of **6a** very slowly due to the mild oxidizing ability of $PhI(OAc)_2$, only ca. 10% conversion was observed after 24 hours. Gratifyingly, under visible light irradiation (λ_{max}= 420 nm), the reaction proceeded much rapidly and the sulfide was smoothly and quantitatively oxidized to corresponding methyl phenyl sulfoxide (**7a**) in high yield and short reaction times (entry 2 in Table 1 and Figure 28). The sulfoxide was the only identifiable oxidation product (> 99% by GC) and the usual undesirable over-oxidation of **7a** to methyl phenyl sulfone (**8a**) was not observed, which manifests the high chemoselectivity of this reaction.

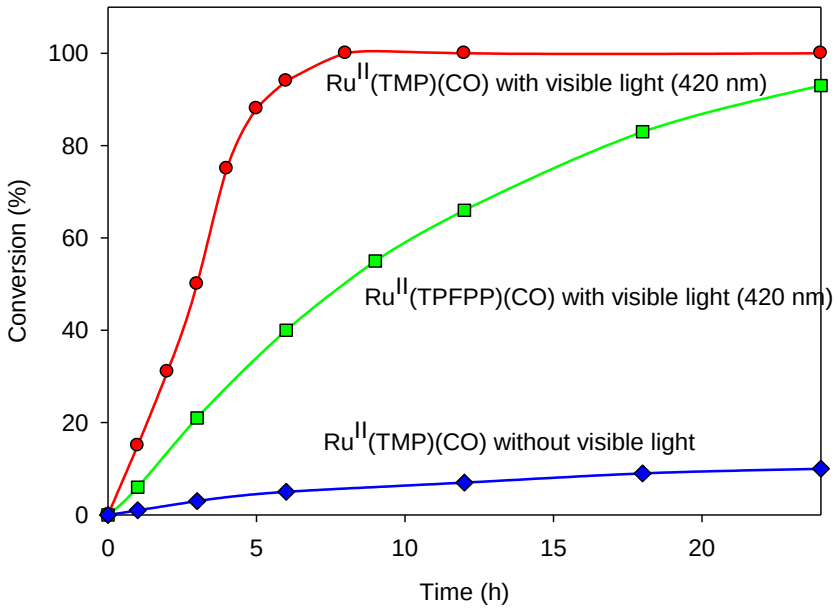

Figure 28. Time courses of oxidation of thioanisole (0.5 mmol) with $PhI(OAc)_2$ (0.75 mmol) in $CDCl_3$ (2 mL) at room temperature catalyzed by **2** (1 μmol): Ru^{II}(TMP)(CO) (**2a**) without visible light (diamond); Ru^{II}(TMP)(CO) (**2a**) with visible light (circle); Ru^{II}(TPFPP)(CO) (**2b**) with visible light (cube). Aliquots were taken at selected time intervals for product analyses with ^{1}H-NMR.

It has been well established that ruthenium(II) carbonyl porphyrins undergo photo-induced decarbonylation reactions.[71] The observed remarkable photo-acceleration with visible light was consistent with photoejection of the carbonyl ligand to generate the ruthenium(II) porphyrin that is much more active form of catalyst to react with the $PhI(OAc)_2$. Therefore, all reactions were carried out under visible light irradiation in a Rayonet photoreactor. The control experiments show that no formation of sulfoxide (< 5%) was detected when the reaction was carried out under light irradiation in the absence of either ruthenium porphyrin catalyst or $PhI(OAc)_2$. In addition, monitoring catalytic

reaction by UV-vis spectroscopy indicated that the no significant degradation of porphyrin catalyst was observed after 24 hour photolysis of visible light.

Table 1. Catalytic oxidation of thioanisole by ruthenium porphyrins with iodobezene diacetate under visible light irradiation[a].

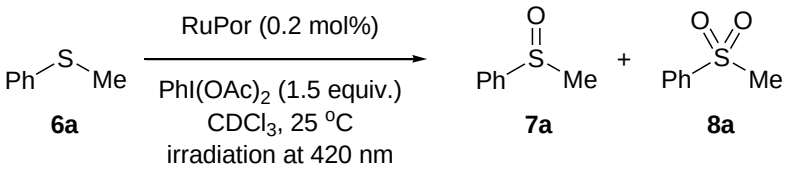

Entry	Catalyst	t (h)	Conv (%)[b]	Mb (%)[b]	Selectivity (**7a : 8a**)[b]
1[c]	$Ru^{II}(TMP)(CO)$	24	10	> 95	> 99 : 1
2		6	94	> 95	> 99 : 1
3[d]		4	100	> 95	> 99 : 1
4[e]		6	61	> 95	> 99 : 1
5[f]		6	92	> 95	> 99 : 1
6	$Ru^{IV}(TMP)Cl_2$	24	< 5	> 95	n.d.
7	$Ru^{VI}(TMP)O_2$	24	15	> 95	95 : 5
8	$Ru^{II}(TPFPP)(CO)$	24	90	> 95	> 99 : 1

[a] All reactions were performed with visible light irradiation (λ_{max}= 420 nm) in a Rayonet reactor or otherwise noted. Reactions were carried out in $CDCl_3$ at ca. 25 °C with a 1:1.5 molar ratio of thioanisole versus $PhI(OAc)_2$ and 0.2 mol% catalyst at an initial substrate concentration of 0.25 M.

[b] Conversions (Conv), mass balance (Mb) and product selectivity were determined by ^{1}H-NMR (JEOL 500M) and/or quantitative GC-MS analysis with an internal standard (diphenylmethane) on the crude reaction mixture after the reaction is quenched by sodium hydroxide solution (consuming all oxygen source).

[c] Without visible light irradiation.

[d] 2 equivalent of $PhI(OAc)_2$ (1 mmol) was used.

[e] 0.4 mol% catalyst.

[f] in CD_2Cl_2.

As expected, the catalytic activity (100% conv. in 4 h) was enhanced with more $PhI(OAc)_2$ present (Table 1, entry 3). The catalytic oxidation was slowed down slightly with double amount of catalyst (0.4 mol%) because of less transmission of visible light (entry 4). Instead of $CDCl_3$, the use of CD_2Cl_2 as the solvent resulted in a similar yield (entry 5). The reaction was also carried out in other solvents like acetonitrile, benzene, diethyl ether, ethyl acetate, hexane, toluene, tetrahydrofuran (THF). Due to the poor solubility of $PhI(OAc)_2$ in all these cases, much slower reactions were obtained with up to 30% conversions (data not shown). In terms of different oxidation state forms of ruthenium catalysts, strikingly, the $Ru^{IV}(TMP)Cl_2$ proved to be completely inactive in the sulfoxidation reaction (entry 6). Much lower conversion was also observed in the oxidation of thioanisole catalyzed by $Ru^{VI}(TMP)O_2$ (entry 7). These results indicate that ruthenium(IV) and ruthenium(VI) are not accessible for the generation of active intermediate in the catalytic oxidation of sulfides by $PhI(OAc)_2$. The electron-efficient catalyst $Ru^{II}(TPFPP)(CO)$ (**2b**), which has been used a robust catalyst in many oxidation reactions, also gave exclusively the sulfoxide, but a longer reaction time (24 h) was necessary for complete substrate conversion (entry 8). More electron-withdrawing groups on porphyrin ligand reduce the reactivity of the catalyst **2b** with $PhI(OAc)_2$ (rate-determining step).

3.2.2 Comparison of various oxygen sources in the catalytic oxidation of thioanisole

A screening of diverse oxygen sources under identical experimental conditions proved that the mild oxygen source $PhI(OAc)_2$ was especially effective and remarkable in the ruthenium(II) porphyrin-catalyzed selective oxidation of sulfide to sulfoxide. The representative results are shown in Table 2. The use of stronger oxidizing oxygen source

like iodosylbenzene (PhIO), *m*-chloroperoxybenzoic acid (*m*-CPBA) or *tert*-butly hydroperoxide (TBHP) gave quantitative conversions with undesirable sulfone formation (Table 2, entries 2-4). The most likely explanation is that these oxygen sources with more oxidizing abilities might generate more reactive oxidizing intermediate with ruthenium porphyrin catalyst.[55, 72] Similar to the catalytic expoxidation of unfunctionlized alkenes,[65] 2,6-dichloropyridine *N*-oxide (2,6-Cl_2PyNO) as the oxygen source afforded excellent selectivity for sulfoxide, however, with a low conversion of 33% after 24 hours (entry 5). Besides the high chemoselectivity, no degradation of the ruthenium porphyrin catalysts was found with $PhI(OAc)_2$ compared to the other oxidants.

Table 2. Catalytic oxidation of thioanisole by ruthenium(II) poprhyrin (**2a**) with various oxygen sources in the presence of visible light[a].

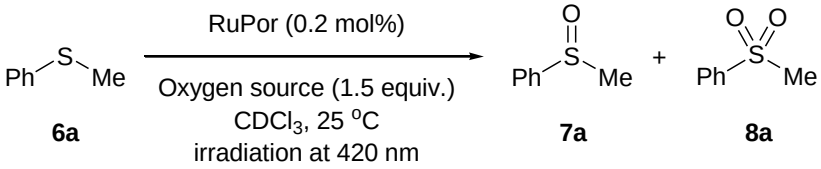

6a **7a** **8a**

Entry	Catalyst	t (h)	Conv (%)[b]	Mb (%)[b]	Selectivity (**7a : 8a**)[b]
1	$PhI(OAc)_2$	6	94	> 95	> 99 : 1
2	PhIO	12	89	96	91 : 9
3	*m*-CPBA	12	100	92	45 : 55
4	TBHP	12	90	> 95	93 : 7
5	2,6-Cl_2PyNO	24	33	> 95	> 99 : 1

[a] All reactions were performed with visible light irradiation (λ_{max} = 420 nm) in a Rayonet reactor. Reactions were carried out in $CDCl_3$ at ca. 25 °C with a 1:1.5 molar ratio of thioanisole versus oxygen source and 0.2 mol% catalyst at an initial substrate concentration of 0.25 M.

[b] Conversions (Conv), mass balance (Mb) and product ratios were determined by ^{1}H-NMR (JEOL 500M) or by quantitative GC-MS analysis with an internal standard (diphenylmethane) on the crude reaction mixture after the reaction is quenched by sodium hydroxide solution (consuming all oxygen source).

3.2.3 Catalytic oxidation of substituted thioanisoles and allylic sulfides by $PhI(OAc)_2$

The substrate scope of the unprecedented catalytic sulfoxidations was explored under optimized conditions. Table 3 lists the oxidized products and corresponding selectivities using the **2a** and **2b** as the catalyst, respectively. In analogy with what we observed for **6a**, all catalytic oxidation of substituted thioanisoles proceeded with a quantitative conversion into the corresponding sulfoxides with excellent selectivity (100%) and mass balance (>95%), and in all cases no traces of sulfones were detected. Significant for preparative purposes, the reactions gave comparable yields in isolated products (entries 1 and 7).

Table 3. Catalytic oxidation of substituted thioanisoles by ruthenium porphyrin (**2**) and $PhI(OAc)_2$ with visible light[a].

Entry	Catalyst **2**	Substrate **6**	Product **7**	t (h)	Conv (%)[b]	yield (%)[b]
1	Ru^{II}(TMP)(CO) **2a**	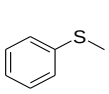	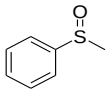	8	100	100 (90)[c]
2		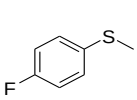	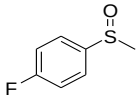	6	100	100
3		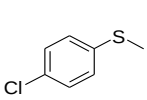	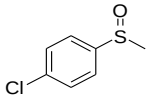	8	100	100
4		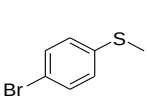	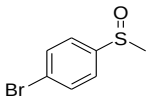	12	100	100
5		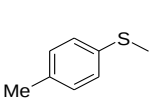	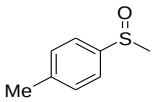	5	100	100
6		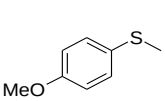	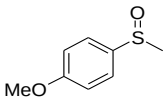	4	100	100
7	Ru^{II}(TPFPP)(CO) **2b**	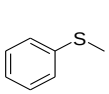	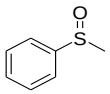	24	100	100 (93)[c]
8		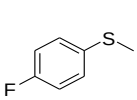	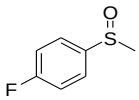	6	100	100
9		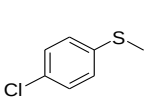	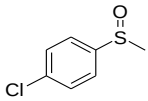	8	100	100
10		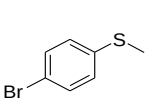	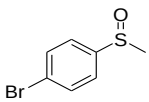	12	90	100
11		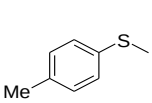	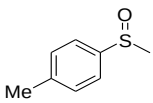	6	100	100
12		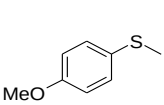	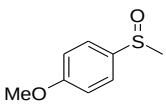	6	100	100

[a] Unless otherwise specified, all reactions were performed in $CDCl_3$ (2 mL) at ca. 25 ^oC with 1.5 equiv. of $PhI(OAc)_2$ (0.75 mmol), substrate (0.5 mmol), 0.2 mol% catalyst, and visible light irradiation (λ_{max} = 420 nm) in a Rayonet reactor; only sulfoxide was detected by ^{1}H-NMR analysis of the crude reaction mixture.
[b] Based on the conversion of thioanisoles and determined by ^{1}H-NMR analysis of the crude reaction mixture; material balance > 95%.
[c] Isolated material after silica-gel chromatography with methylene and n-hexane as eluent.

We also followed the time courses of oxidation of *para*-substituted thioanisoles by Ru^{II}(TMP)(CO) (**2a**) and $PhI(OAc)_2$ under visible light photolysis (Figure 29). The introduction of electron-donating and electron-withdrawing substituents in the aryl ring of substrates gave the noticeable effect. As is evident, the introduction of electron-donating groups like methyl or methoxy groups resulted in increased reactivities compared to thioanisole (entries 5, 6, 11, 12), while reduced reactivities were observed in the presence of electron-withdrawing groups like Cl or Br groups (entries 3, 4, 9, 10). The stoichiometric thioanisoles oxidation by *trans*-dioxoruthenium(VI) porphyrins exhibits a nonlinear Hammett relationship, in which case both electron-donating and -withdrawing substituents moderately slow down the reactions.[73] Apparently, involvement of *trans*-dioxoruthenium(VI) species as the premier reactive intermediate is implausible.

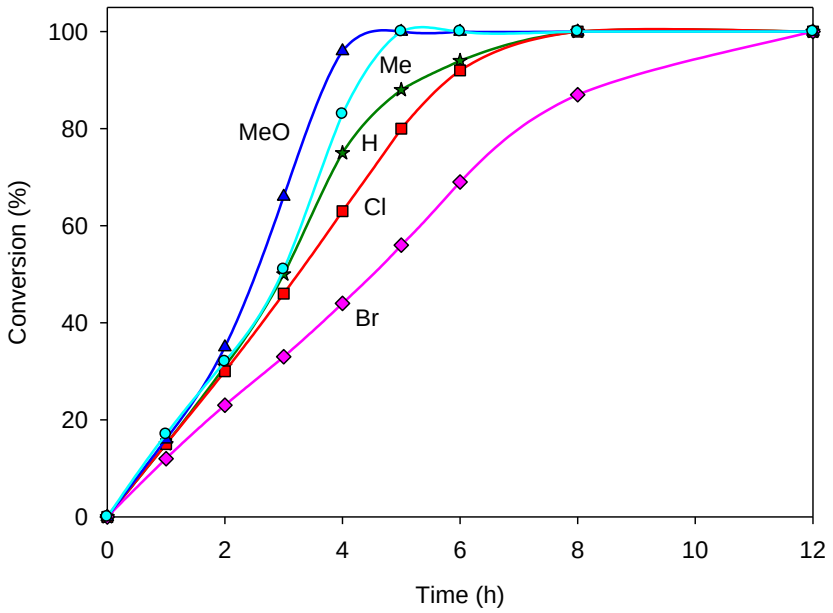

Figure 29. Time courses of oxidation of para-substituted (4-X) thioanisoles (0.5 mmol) with $PhI(OAc)_2$ (0.75 mmol) in $CDCl_3$ (2 mL) at ca. 25 ^oC catalyzed by **2a** (1 μmol) under visible light irradiation. X = H (star), MeO (triangle), Me (circle), Cl (square) and Br (diamond).

The present results demonstrate that the ruthenium porphyrin with $PhI(OAc)_2$ is an efficient catalytic system for the selective oxidation of sulfides. Its efficacy for epoxidation was also tested with unfunctionalized *cis*-cyclooctene under the optimized reaction conditions. Surprisingly, no appreciable reactivity (<1% conv.) was observed after 24 h under identical reaction conditions. This result stimulates us to test the oxidation of allylic sulfides. The oxidation of sulfides in the presence of electron-rich double bonds is often problematic with many traditional oxidants such *m*-CPBA, $NaIO_4$, and catalytic systems because of interference with epoxidations.[48] With ruthenium(II) catalyst and $PhI(OAc)_2$, no epoxidation took place and excellent chemoselectivities for

sulfoxide were obtained with somewhat low reactivities (Table 4). Similarly, presence of hydroxy group did not interfere with the selective oxidation of sulfide to sulfoxide and no alcohol oxidation was detected (entry 3 in Table 4).

Table 4. Catalytic oxidation of allylic or hydroxy sulfides by ruthenium porphyrin (**2**) and $PhI(OAc)_2$ with visible light[a].

Entry	Catalyst **2**	Substrate **6**	Product **7**	Conv (%)[b]	Yield (%)[b]
1	Ru^{II}(TMP)(CO) **2a**	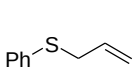	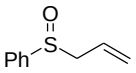	40	100
2		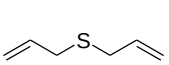	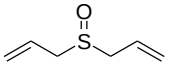	62	100
3[c]		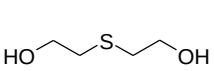	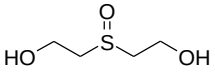	100	100
4	Ru^{II}(TPFPP)(CO) **2b**	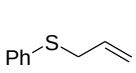	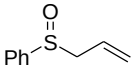	32	100
5		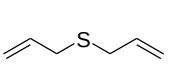	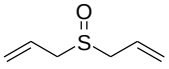	64	100

[a] Unless otherwise specified, all reactions were performed in $CDCl_3$ (2 mL) at ca. 25 ^oC with 1.0 equiv. of $PhI(OAc)_2$ (0.5 mmol), substrate (0.5 mmol), 0.2 mol% catalyst, and visible light irradiation (λ_{max} = 420 nm) in a Rayonet reactor; only sulfoxide was detected by ^{1}H-NMR analysis of the crude reaction mixture.
[b] Based on the conversion of thioanisoles and determined by ^{1}H-NMR analysis of the crude reaction mixture; material balance > 95%. The products were fully characterized after column chromatography.
[c] 1.5 equiv. of $PhI(OAc)_2$ was used.

3.3 Mechanistic studies of transient oxidizing species

Prior to the present studies, the use of ruthenium porphyrins for catalytic sulfoxidations has limited success due to the low reactivity and undesirable over-oxidation to sulfones in most cases. We now show that ruthenium porphyrins catalyze the

highly selective oxidation of substituted thioanisoles and allylic sulfides by $PhI(OAc)_2$ in the presence of visible light. The preparative utility and synthetic value of the new catalytic system presented above is indisputable, but mechanistic understanding of the complex oxygen-transfer processes is important for the design of more effective and selective oxidants with general applicability.

In fact, *trans*-dioxoruthenium(VI) porphyrin is capable of oxidizing epoxidation or hydroxylation and undergoes reduction in the presence of olefins or alcohols.[18] However, ruthenium porphyrin and $PhI(OAc)_2$ system is inert towards expoxidation or hydroxylation in the catalytic oxidation of allylic and hydroxy sulfides strongly suggests that *trans*-dioxoruthenium(VI) porphyrin is not a viable oxidizing intermediate in above catalytic cycle, even if it does have the ability to effect substrate oxidations.

To prove this point further, the competitive sulfoxidation reactions catalyzed by carbonyl ruthenium(II) porphyrin complexes (**2**) with $PhI(OAc)_2$ were conducted as described experimental section. The purpose of the competition studies is to evaluate whether the same species of metal-oxo intermediate was active in two different sets of conditions by comparing the ratios of products formed under catalytic conditions to the ratios of the rate constants measured in direct kinetic studies.[74] If the same metal-oxo intermediate was present in both cases, the relative ratios of absolute rate constants from direct kinetic measurements and relative rate constants from the competition studies should be similar,[41] although a coincident similarity for two different oxidants could not be excluded. When the ratios were not similar, however, the active oxidants under the two sets of conditions must be different.[73, 75]

Table 5 contains the results of kinetic results with *trans*-dioxoruthenium(VI) porphyrin complexes from our recent study[73] and competition reactions where $PhI(OAc)_2$ was employed as sacrificial oxidant, respectively. Each sulfide substrate was oxidized to the corresponding sulfoxide in nearly quantitative yield based on the oxidant consumed. In this study, a limiting amount of $PhI(OAc)_2$ was used to keep the conversion less than 20% in the purpose of reducing potential problems in product analysis due to secondary oxidations and multiple oxidation products. In most cases, the ratios of absolute rate constants found in direct kinetic studies differed from the oxidation ratios for competition oxidation reactions of the two substrates, as evident in Table 5. These results from the competition studies suggest that an unusually different behavior is apparent during catalytic turnover conditions with ruthenium(II) catalysts. The differences appear to be statistically significant in the ratios of substrate oxidation rates. The oxidation rate ratios for each pair of substrates were found to be much more larger (more selective) when $PhI(OAc)_2$ employed compared to that from the absolute rate constants ratio of $Ru^{VI}(Por)O_2$, implying also that the active oxidant generated under catalytic turnover condition with $PhI(OAc)_2$ should be less reactive than $Ru^{VI}(Por)O_2$. Therefore, a *trans*-dioxoruthenium(VI) porphyrins are unlikely to be the active oxidant under turnover conditions.

Table 5. Comparison of competition catalytic oxidations with ratios of absolute rate constants of *trans*-dioxoruthenium(VI) porphyrins[a].

Porphyrin System	Substrates	Method	k_{rel}[b]
TPFPP	*p*-fluorothioanisole/thioanisole	kinteic results $PhI(OAc)_2$	0.94 1.49
TPFPP	*p*-chlorothioanisole/thioanisole	kinteic results $PhI(OAc)_2$	0.71 3.22
TPFPP	*p*-methylthioanisole/thioanisole	kinteic results $PhI(OAc)_2$	0.66 2.23
TPFPP	*p*-methoxythioanisole/thioanisole	kinteic results $PhI(OAc)_2$	0.64 3.70
TMP	*p*-fluorothioanisole/thioanisole	kinteic results $PhI(OAc)_2$	0.38 1.47
TMP	*p*-chlorothioanisole/thioanisole	kinteic results $PhI(OAc)_2$	1.01 3.12

[a] A reaction solution containing equal amounts of two substrates, e.g., thioanisole (0.5 mmol) and substituted thioanisole (0.5 mmol), $PhI(OAc)_2$ (0.4 mmol), ruthenium(II) porphyrin catalyst (1 μmol) and an internal standard of diphenylmethane (0.1 mmol) was prepared in CH_3Cl (5 mL) and the mixture was stirred overnight (12 h) under visible light irradiation at 25 ± 2 ^oC.

[b] Relative ratios of absolute rate constants from kinetic results with *trans*-dioxoruthenium(VI) porphyrin complexes and for competitive oxidations with carbonyl ruthenium(II) porphyrin catalysts (**2a** and **2b**). All competition ratios are averages of 2-3 determinations with standard deviations smaller than 10% of the reported values.

To further probe the nature of the transient oxidizing species, we conducted the chemical oxidation reaction of ruthenium(II) catalyst **2** by $PhI(OAc)_2$ in $CHCl_3$ in the absence of sulfides (Figure 30). As shown in Figure 30 (A), with five equivalent of $PhI(OAc)_2$, the precursor Ru^{II}(TMP)(CO) (**2a**) was quantitatively converted to a species **9a** with a blue shift of the weak Soret band at 406 nm, red shift of broad absorption bands around 550-750 nm, and with clearly resolved isosbestic points. The absorption spectrum

of **9a** was essentially identical to that of the known ruthenium(IV) mono-oxo porphyrin. **9a** can also produced by reduction of $Ru^{VI}(TMP)O_2$ with excess *cis*-cylcooctene (Figure 31).[55] As shown in Figure 30(B), further addition of $PhI(OAc)_2$ up to a total of 20 equivalent resulted in conversion of **2a** to another species **10a** with a red shift of the Soret band to 422 nm and blue shift of Q band to 518 nm, again with clean isosbestic points. The later signal of the final product is characteristic of the well-known *trans*-dioxoruthenium(VI) poprhyrin, i.e. $Ru^{VI}(TMP)O_2$.[72] These results unambiguously demonstrate that $PhI(OAc)_2$ can be used as a single oxygen atom source in generating *trans*-dioxoruthnium(VI) porphyrin via a monoruthenium(IV)-oxo intermediates (Eq. 1.). Of note, the formation of *trans*-dioxoruthenium(VI) porphyrin species (**10a**) was not observed for the same reaction but in the presence of organic sulfides.

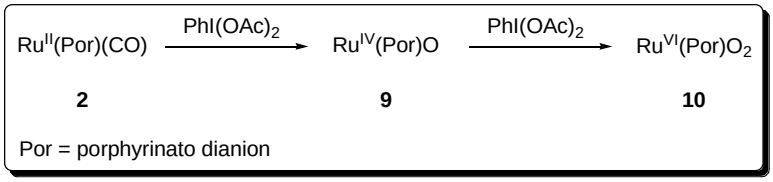

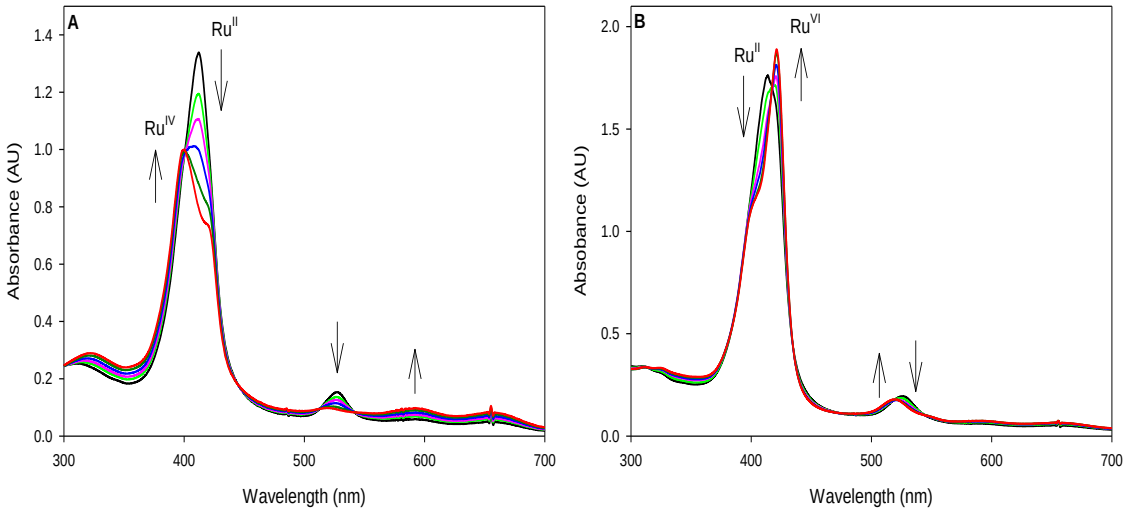

Figure 30. Time-resolved spectra for the oxidation of **2a** (5×10^{-6} M) with $PhI(OAc)_2$ in $CHCl_3$. (A) 5 equivalent of $PhI(OAc)_2$ over 40 min. (B) 20 equivalent of $PhI(OAc)_2$ over 20 min.

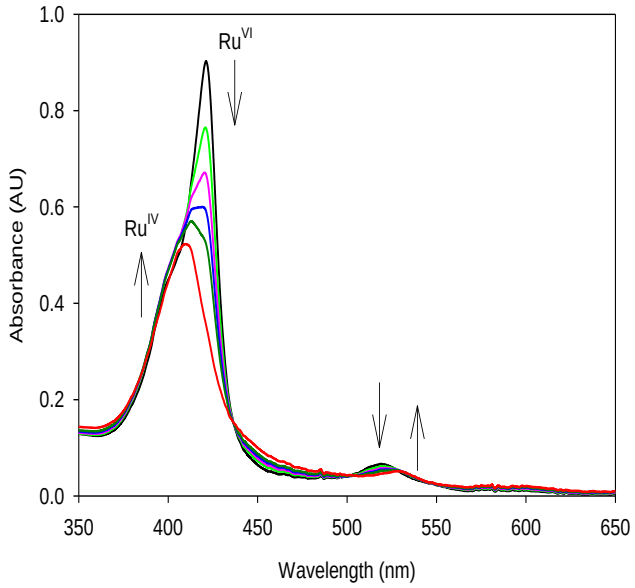

Figure 31. Time-resolved spectrum in the reduction of $Ru^{VI}(TMP)O_2$ (8×10^{-6} M) to $Ru^{IV}(TMP)O$ in the presence of excess *cis*-cyclooctene in $CHCl_3$ solution at 23 ^oC over 2 h.

The second-order rate constants for the formation of **10a** was also measured with different concentration of $PhI(OAc)_2$ under pseudo first-order conditions. A k_2 value of 14.31×10^3 $M^{-1}s^{-1}$ was obtained from the slope of linear fit (Figure 32).

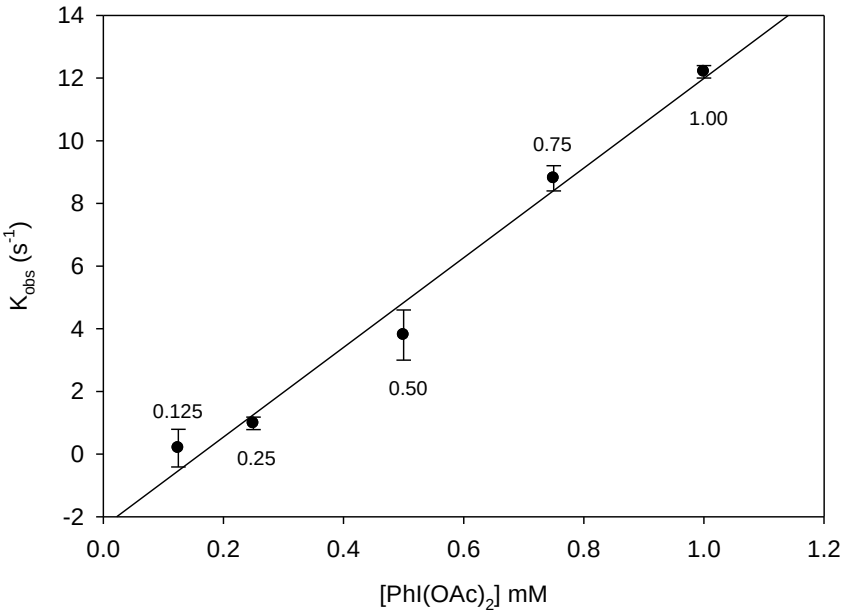

Figure 32. Kinetic plot of the reaction of **2a** (5×10^{-6} M) with $PhI(OAc)_2$ in $CHCl_3$ at 0.125 mM, 0.25 mM, 0.5 mM, 0.75 mM, 1.0 mM ($k_2 = 14.31 \times 10^3$ $M^{-1}s^{-1}$, R = 0.9826).

It is well known that ruthenium(IV)-oxo porphyrins are much less reactive than the corresponding *trans*-dioxoruthenium(VI) porphyrins as the latter can oxidize the alkenes to expoxides and the former does not oxidize the alkenes but react with powerful reductants like triphenylposphine.[76] Similarly, the electron-deficient $Ru^{VI}(TPFPP)O_2$ (**10a**) with Soret band at 412 nm and Q band at 506 nm can be prepared by oxidation of the carbonyl precursor **2b** with 30 equivalent of $PhI(OAc)_2$, as shown by the close spectral agreement with the TMP analogue (Figure 33). Due to the electron-demanding nature, the oxidation of $Ru^{II}(TPFPP)(CO)$ to $Ru^{VI}(TPFPP)O_2$ is much slower than that of TMP analogue.

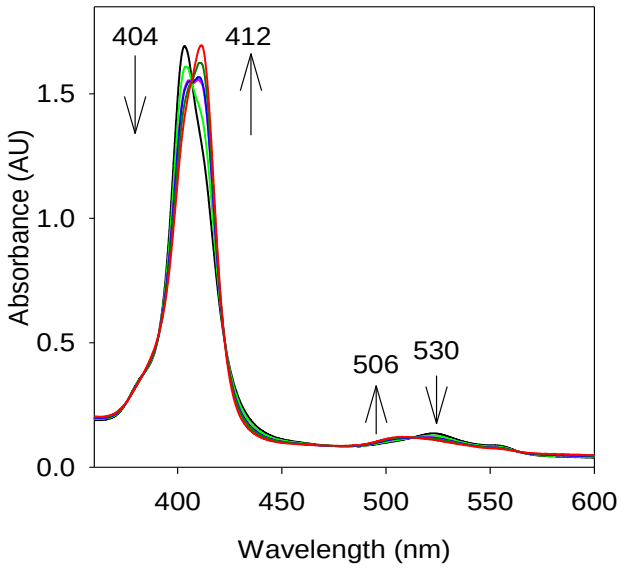

Figure 33. UV-visible spectral changes observed in the reactions of Ru^{II}(TPFPP)(CO) to Ru^{VI}(TPFPP)O_2 (6×10^{-6} M) in the presence of $PhI(OAc)_2$ (30 equivalent) in $CHCl_3$ solution at 23 ^{o}C over 30 min.

On the basis of the present experimental facts, a catalytic cycle is proposed in Scheme 14. First, visible light photolysis of carbonyl **2** gives a more active ruthenium(II) species Ru^{II}Por. Second, oxidation of Ru^{II}Por with $PhI(OAc)_2$ generated the ruthenium(IV)-oxo porphyrin (**7**) as the major oxidizing intermediate which subsequently oxidizes an organic sulfide selectively to sulfoxide in view of its low reactivity. After the oxygen transfer from the ruthenium(IV)-oxo species **9** to the sulfide, the precursor Ru^{II}Por (Scheme 14) was reformed. The critical formation of the low-reactivity ruthenium(IV)-oxo poprhyrin was unequivocally confirmed by the oxidation of **2a** with $PhI(OAc)_2$ in the absence of sulfide substrate (Figure 30A). The notable absence of reactivity in the case of expoxidation and hydroxylation compared to sulfoxidation for the

oxidation of allylic or hydroxy sulfides illustrates that the formation of more reactive *trans*-dioxoruthenium(VI) species is not directly involved in above catalytic cycle.

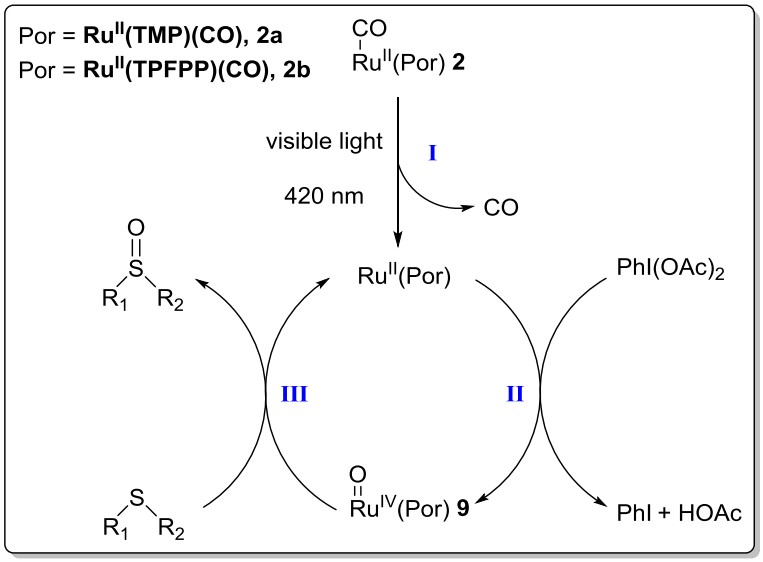

Scheme 14. A proposed catalytic cycle for the photocatalytic oxidations by the ruthenium(II) carbonyl porphyrin in the presence of $PhI(OAc)_2$ and visible light.

4. CATALYTIC OXIDATIONS BY IRON CORROLES

4.1 Introduction

Photochemical reactions are intrinsically advantageous because activation is obtained by the absorption of a photon, which leaves no residue; whereas most chemical methods involve the use of toxic/polluting reagents.[77] To this end, we aim to use visible light (sunlight) to induce reversible redox processes of the metal center, avoiding all the disadvantages deriving from the use of chemical reagents. The chemistry of cofacial bisporphyrins has also drawn increased attention owing to the ability of these systems to utilize molecular oxygen and visible light for organic oxidations.[78-79] One example is the catalytic aerobic oxidation by high-valent iron(IV)-oxo species in a process that involves photo-disproportionation of a diiron(III)-μ-oxo bisporphyrin complex.[80-81] The low reactivity of the formed iron(IV)-oxo oxidant and the poor quantum efficiency are serious obstacles that prohibit the use of iron porphyrins as practical photocatalysts.

4.2 Visible light-driven aerobic oxidation catalyzed by a diiron(IV) μ-oxo biscorrole complex

Recently, we have reported that ruthenium(IV) μ-oxo bisporphyrins catalyze the aerobic oxidation of hydrocarbons through a ruthenium(V)-oxo species in a photo-disproportionation mechanism.[82] Another way to investigate the scope of the photo-disproportionation reactions could be the utilization of corrole complexes with iron metal. Our studies have shown that the photochemistry of a fluorinated iron(IV) μ-oxo biscorrole appears to present a photo-disproportionation manifold similar to that of the iron porphyrin systems.[83] In this section, we describe a visible-light driven aerobic

oxidation of hydrocarbons catalyzed by a biscorrole-iron(IV) μ-oxo complex using only molecular oxygen without the need for an external reducing reagent. The proposed catalytic sequence involves the following: (1) photo-disproportionation of the μ-oxo iron(IV) biscorrole to form iron(III) and iron(V)-oxo oxidizing species; (2) substrate oxidation by resulting iron(V)-oxo species to give oxidized products and a second iron(III) species; (3) aerobic oxidation of iron(III) complex to regenerate the μ-oxo iron(IV) dimer.

Similar to the well-established photo-disproportionation of diiron(III)-μ-oxo bisporphyrin complexes,[80] we probed the irradiation of the thermally stable complex **5b** with visible light in the presence of excess triphenylphosphine (4 mM), which converted **5b** to iron(III) corrole monomer (**4b**) with well-anchored isosbestic points (Figure 34). The reactants and products of the overall photoreaction (depicted in the inset) are matched to their respective absorption profiles.[84] This photochemical observation of a clean reduction of $[Fe^{IV}(TPFC)]_2O$ to $Fe^{III}(TPFC)$ supports a photo-disproportionation pathway that allows for the generation of the iron(V)-oxo oxidant. Similar spectral changes were also observed upon the photolyses of diruthenium(IV)-μ-oxo bisporphyrin complexes in the presence of excess Ph_3P.[82]

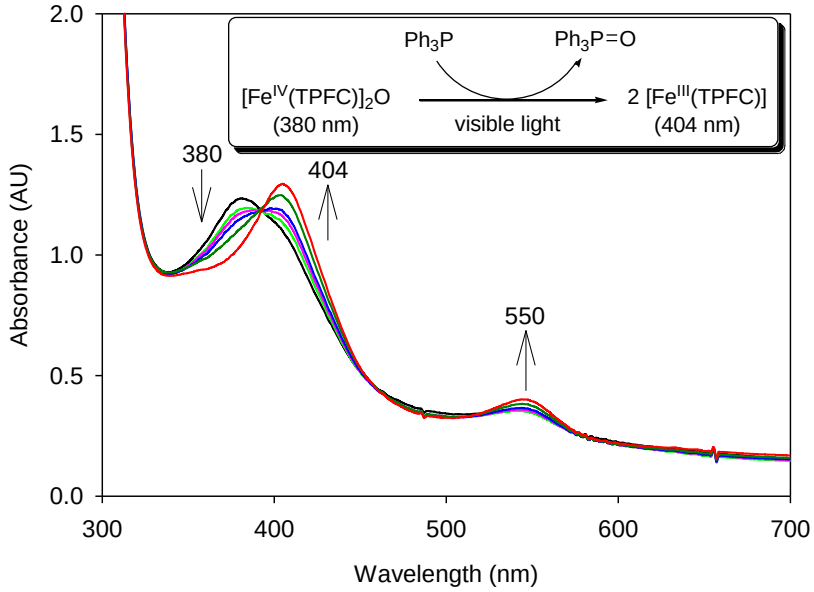

Figure 34. UV–visible spectral change of $[Fe^{IV}(TPFC)]_2O$ (**5b**) in the presence of Ph_3P (4 mM) upon irradiation with a visible lamp (λ_{max}= 420 nm) in anaerobic CH_3CN solution over a span of 15 min at 2 min intervals.

4.2.1 Screening catalytic oxidations of *cis*-cyclooctene

As shown in the Figure 32, the photo-disproportionation reaction of diiron(IV)-μ-oxo biscorrole (**5b**) becomes catalytic in the presence of O_2. First, the efficacy of photo-disproportionation of μ-oxo iron(IV)biscorrole (**5b**) for a light-driven oxidation catalysis was evaluated in the aerobic oxidation of *cis*-cyclooctene (Table 6). Our immediate goal in this section was to identify the most efficient systems and optimal conditions from the screening reactions. After 24 h of photolysis with visible light (λ_{max}= 420 nm), *cis*-cyclooctene oxide was obtained as the only identifiable oxidation product (> 95% by GC) with ca. 90 turnovers (abbreviated as TON, representing moles of product/moles of catalyst) of catalyst **5b** (entry 1). The trend in the TONs roughly paralleled irradiation

times and up to 540 TONs was obtained after four day irradiation. Control experiments showed that no epoxide was formed in the absence of either the catalyst or light (data not shown). The use of other solvents instead of CH_3CN resulted in reduced TONs (entries 2–4), presumably due to a slower formation of the dimeric precursor **5b**. It is known that the transformation of **4b** to its μ-oxo dimer **5b** has a very large solvent effect.[84] Catalyst degradation was a serious problem with higher-energy light and the use of UV irradiation (λ_{max}= 350 nm) shut down the catalytic activity completely (entry 5). Monitoring reaction by UV–vis spectroscopy indicated that the corrole catalyst was completely degraded only after 30 min photolysis of UV light.

In order to gain insight into the possible contribution of the radical autooxidation to the observed photocatalytic process, the experiment was also carried out in the presence of radical scavenger. Of note is the well-known radical scavenger *N*-*tert*-butyl-phenylnitrone had almost no effect on cyclooctene epoxide formation (entry 7), which implies a non-radical oxidation process. It is interesting to note that the catalytic activity was enhanced by adding small amount of anthracene (entries 6 and 9), which could act as a photosensitizer. Similar enhancement effect was observed in the ruthenium(IV) μ-oxo bisporphyrins system.[82] In addition, the monomeric iron corrole Fe^{III}(TPFC) was tested as photocatalyst, which is capable of in situ formation of the μ-oxo dimer, giving comparable activity (entries 8 and 9). Instead, non-halogenated Fe^{III}(TPC) did not show appreciable catalytic activity under identical conditions (entry 10). Clearly, the formation of μ-oxo dimer by molecular oxygen is essential for reactivity in the photocatalytic epoxidation of *cis*-cyclooctene. For the purpose of comparison, the well-known diiron(III) μ-oxo bisporphyrin complex $[Fe^{III}(TPP)]_2O$ and *trans*-dioxoruthenium(VI)

tetramesityporphyrin, i.e. $Ru^{VI}(TMP)O_2$, were also evaluated under identical conditions, giving comparatively low activities (entries 12 and 13).

Table 6. Photocatalytic aerobic oxidation of *cis*-cyclooctene by a diiron(IV) μ-oxo biscorrole[a].

Entry	Catalyst	Solvent	T (day)	TON[b, c]
1	$[Fe^{IV}(TPFC)]_2O$	CH_3CN	1	90 ± 10
			2	200 ± 12
			3	320 ± 30
			4	540 ± 40
2		$CHCl_3$	1	34 ± 5
3		C_6H_6	1	60 ± 10
4		THF	1	70 ± 9
5[d]		CH_3CN	1	< 10
6[e]		CH_3CN	1	140 ± 16
7[f]		CH_3CN	1	81 ± 10
8	$[Fe^{III}(TPFC)]\cdot Et_2O$	CH_3CN	1	85 ± 5
9[e]		CH_3CN	1	154 ± 26
10	$[Fe^{III}(TPC)]\cdot Et_2O$	CH_3CN	1	n.d.
11	$[Fe^{III}(TPP)]_2O$	CH_3CN	1	40 ± 5
12	$Ru^{VI}(TMP)O_2$	CH_3CN	1	18 ± 2

[a] The reaction was carried out in a Rayonet reactor, with ca. 0.5 μmol of catalyst in 5 mL of solvent containing 4 mmol of *cis*-cyclooctene. Oxygen-saturated solutions were irradiated with visible light (λ_{max}= 420 nm) or otherwise noted. Products were analyzed on an HP 6890 GC with a DB-5 capillary column employing an internal standard (1,2,4-trichlorobenzene).
[b] TON represents the total number of moles of product produced per mole of catalyst. All reactions were run 2–3 times, and the data reported are the averages with standard deviation (1σ). Note the product yields in our catalytic studies are not given because we typically have large excesses of substrates to catalyst (>8000:1).
[c] The major product was *cis*-cyclooctene oxide, detected in >95% yield.

[d] UV light (λ_{max} = 350 nm).
[e] 5 mg of anthracene was added.
[f] 5 mg of *N*-*tert*-butyl-phenylnitrone (radical inhibitor) was added.

4.2.2 Photocatalytic aerobic oxidation of alkenes and activated hydrocarbons

To further explore the substrate scope of the diiron(IV) μ-oxo corrole catalyst, the photocatalytic oxidations of a variety of organic substrates were examined under visible light and optimized conditions. Table 7 lists the oxidized products and corresponding TONs using the **5b** as the photocatalyst. The trend in the TONs roughly parallels the substrate reactivity and significant activity was observed with up to 1580 TON. Similar to *cis*-cyclooctene, norborbene was oxidized to corresponding epoxide (*exo* mainly) with 72 TON after 24 h photolysis (entry 1). Cyclohexene, in contrast, which is susceptible to the allylic oxidation, gave primarily 2-cyclohexenol and 2-cyclohexenone along with minor expoxide (entry 2). This product distribution is no different than those typically obtained from cofacial iron and ruthenium porphyrin photocatalysts.[85] Activated hydrocarbons including triphenylmethane, diphenylmethane, ethylbenzene and xanthenes were oxidized to the corresponding alcohols and/or ketones from overoxidation with total TONs ranging from 80 to 1200 (entries 3–6). As is evident from Table 7, the oxidation of secondary benzylic alcohols gave the highest catalytic activities (entries 7 and 8).

Table 7. Turnover numbers of photocatalyst **5b** for alkenes and benzylic C-H oxidations[a].

Entry	Substrate	Product	TON[b]
1[c]		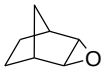	72 ± 6
			40 ± 4
2		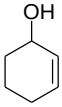	230 ± 24
		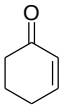	40 ± 16
3[d]	Ph_3CH	Ph_3COH	380 ± 40
4	Ph_2CH_2		702 ± 60
			220 ± 20
5	$PhCH_2CH_3$		80 ± 5
			10 ± 2
6	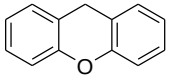	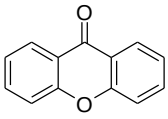	1235 ± 120
7			1300 ± 140
8	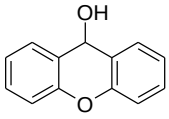	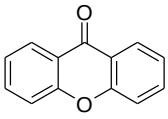	1580 ± 175

[a] Typically with 0.5 μmol of **5b** in 5 mL of CH_3CN containing 4–8 mmol of substrate and 5 mg anthracene.
[b] Determined for a 24 h photolysis (λ_{max}= 420 nm). The values (1σ) reported are the averages of 2–3 runs.
[c] >90% *exo* isomer.
[d] A minor product was detected by GC but not identified.

4.3 Selective sulfoxidations catalyzed by iron(III) corrole complexes

4.3.1 Screening the catalytic oxidation of thioanisole

Ruthenium porphyrin complexes with $PhI(OAc)_2$ showed unprecedented selectivity for catalytic oxidation of sulfides. Thus, in this section, we have also investigated the $PhI(OAc)_2$ as a mild oxygen source in the catalytic oxidation of sulfides (**6a**) with iron corrole catalysts. In order to work under homogeneous conditions and follow the analysis via ^{1}H-NMR, the reactions were performed in CD_3OD at room temperature using a 0.2 mol% catalyst loading and a 1:1.5 ration of thioanisole and $PhI(OAc)_2$. $Fe^{III}(TPC)\cdot(OEt_2)_2$ (**4a**) with $PhI(OAc)_2$ catalyzed the oxidation of **6a** rapidly, giving corresponding methyl phenyl sulfoxide (**7a**) in good yield (entry 1 in Table 8 and Figure 33). The sulfoxide was the only identifiable oxidation product (> 99% by GC) and the usual undesirable over-oxidation of **7a** to methyl phenyl sulfone (**8a**) was not observed.

As expected, the catalytic activity (94% Conv.) was enhanced with more $PhI(OAc)_2$ present (Table 8, entry 2). Instead of CD_3OD, the use of $CDCl_3$ and CD_3CN as the solvent resulted in much lower conversions (entry 3-4). Similar as ruthenium porphyrins system (**2**), the electron-deficient catalyst $Fe^{III}(TPFC)\cdot(OEt_2)_2$ (**4b**) gave relatively low conversion (entry 5). By comparison, diiron(IV)-μ-oxo biscorrole (**5b**) showed low conversion with only 16%. $Ru^{II}(TMP)(CO)$ (**2a**) showed much low activity, and only ca. 10% conversion was observed after 24 hours (entry 7).

Table 8. Catalytic oxidation of thioanisole by catalysts with iodobezene diacetate[a].

Entry	Catalyst	Conv (%)[b]	Mb (%)[b]	Selectivity (**7a** : **8a**)[b]
1	$Fe^{III}(TPC)\cdot(OEt_2)_2$	80	> 95	> 99 : 1
2[c]		94	> 95	> 99 : 1
3[d]		7	> 95	> 99 : 1
4[e]		5	> 95	> 99 : 1
5	$Fe^{III}(TPFC)\cdot(OEt_2)_2$	46	> 95	> 99 : 1
6	$[Fe^{IV}(TPFC)]_2O$	17	> 95	> 99 : 1
7	$Ru^{II}(TMP)(CO)$	10	> 95	> 99 : 1

[a] All reactions were performed in CD_3OD at ca. 25 ^oC with a 1:1.5 molar ratio of thioanisole versus $PhI(OAc)_2$ and 0.2 mol% catalyst at an initial substrate concentration of 0.25 M and the mixture was stirred for 60 minutes
[b] Conversions (Conv), mass balance (Mb) and product selectivity were determined by ^{1}H-NMR (JEOL 500M) and/or quantitative GC-MS analysis with an internal standard (1,2,4-trichlorobenzene) on the crude reaction mixture after the reaction is quenched by sodium hydroxide solution (consuming all oxygen source).
[c] 2 equivalent of $PhI(OAc)_2$ (1 mmol) was used.
[d] in $CDCl_3$.
[e] in CD_3CN.

The effect of water on the catalytic oxidation of **6a** by **4** was investigated and results were summarized in Table 9. In the presence of small amount of H_2O (0.25 equiv.), the sulfoxidation reactions proceeded very rapidly and completely within only 2 minutes (entry 4 and 6). However, undesired **8a** from over-oxidation of **7a** when the amount of H_2O was increased (entry 4-7). Detailed studies will be required to understand the water effect on the catalytic sulfoxidation. One possible speculation is that the more oxidizing PhIO can be formed by the reaction of $PhI(OAc)_2$ with H_2O.[86]

Since we have observed a significant water effect on the rate of sulfoxidation reactions, we followed the time courses of oxidation of thioanisole with $PhI(OAc)_2$ in the presence and absence of H_2O. The results in Figure 35 show that the yield of sulfoxidation completed within 30 minutes in 0.25 mmol of H_2O and 2 minutes in 0.5 mmol of H_2O. Whereas a relative slow formation of sulfoxide was observed when the reaction was carried out in the absence of water and completed within 120 mins. However, the addition of more water reduced the selectivity for **7a**.

Table 9. Catalytic oxidation of thioanisole by $Fe^{III}(TPC)\cdot(OEt_2)_2$ (**4a**) with iodobezene diacetate in the presence of H_2O[a].

Entry	Solvent	H_2O (mmol)	t (min)	Conv (%)[b]	Mb (%)[b]	Selectivity (**7a** : **8a**)[b]
1	CH_3OH	0	2	39	> 95	> 99 : 1
2		0	60	80	> 95	> 99 : 1
3		0	90	93	> 95	> 99 : 1
4		0.25	2	86	> 95	98 : 2
5		0.25	20	93	> 95	98 : 2
6		0.5	2	100	> 95	89 : 11
7		0.5	60	100	> 95	69 : 31
8	$CHCl_3$	0.5	60	67	> 95	> 99 : 1
9	CH_3CN	0.5	60	99	> 95	92 : 8

[a] All reactions were performed in CD_3OD at ca. 25 ^oC with a 1:1.5 molar ratio of thioanisole versus $PhI(OAc)_2$ and 0.2 mol% catalyst at an initial substrate concentration of 0.25 M and the mixture was stirred for 60 minutes

[b] Conversions (Conv), mass balance (Mb) and product selectivity were determined by ^1H-NMR (JEOL 500M) and/or quantitative GC-MS analysis with an internal standard (1,2,4-trichlorobenzene) on the crude reaction mixture after the reaction is quenched by sodium hydroxide solution (consuming all oxygen source).

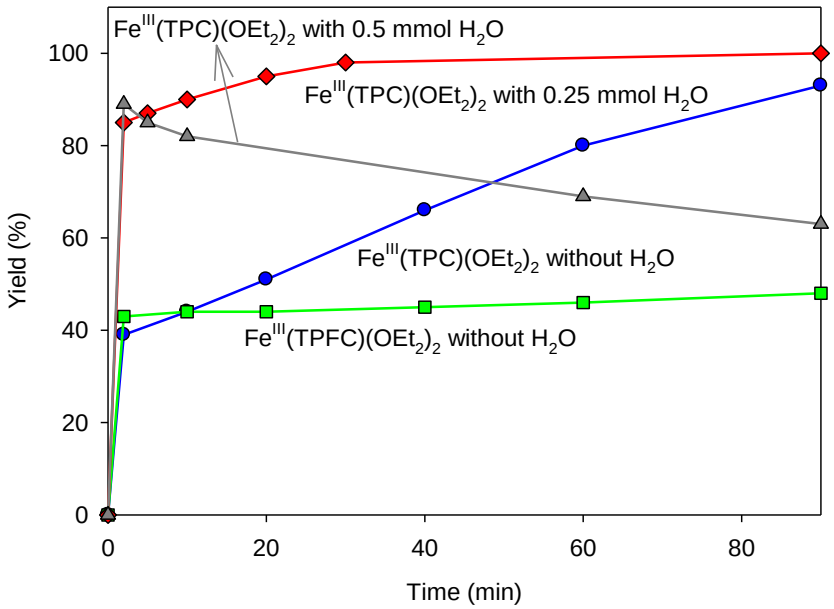

Figure 35. Time courses of oxidation of thioanisole (0.5 mmol) with $PhI(OAc)_2$ (0.75 mmol) in CD_3OD (2 mL) at room temperature catalyzed by **4** (1 μmol): $Fe^{III}(TPC)\cdot(OEt_2)_2$ (**4a**) without H_2O (circle); $Fe^{III}(TPFC)\cdot(OEt_2)_2$ (**4b**) without H_2O (cube); $Fe^{III}(TPC)\cdot(OEt_2)_2$ (**4a**) with 0.25 mmol H_2O (dimond); $Fe^{III}(TPC)\cdot(OEt_2)_2$ (**4a**) with 0.5 mmol H_2O (triangle). Aliquots were taken at selected time intervals for product analyses with ^{1}H-NMR.

4.3.2 Comparison of various oxygen sources in the catalytic oxidation of thioanisole

A screening of diverse oxygen sources under identical experimental conditions proved that the mild oxygen source $PhI(OAc)_2$ was especially effective and remarkable in the iron(III) corrole-catalyzed selective oxidation of sulfide to sulfoxide (Table 10). The use of stronger oxidizing oxygen source like iodosobenzene (PhIO) or *tert*-butylperoxide (TBHP) afforded excellent selectivity to sulfoxide, however, with a very low conversion of 3% and 17% after 60 minutes (Table 10, entries 2-3). *m*-Chloroperoxybenzoic acid (m-

CPBA) gave relatively high conversion with undesirable sulfone formation (entry 4). Notably, these oxygen sources with more oxidizing abilities might accelerate the degradation of the iron corrole catalysts within 30 minutes compared to mild oxidant of $PhI(OAc)_2$.

Table 10. Catalytic oxidation of thioanisole by $Fe^{III}(TPC)\cdot(OEt_2)_2$ (**4a**) with various oxygen sources[a].

Entry	Catalyst	Conv (%)[b]	Mb (%)[b]	Selectivity (**7a : 8a**)[b]
1	$PhI(OAc)_2$	80	> 95	> 99 : 1
2	PhIO	3	> 95	> 99 : 1
3	TBHP	17	> 95	> 99 : 1
4	*m*-CPBA	36	93	77 : 23

[a] All reactions were carried out in CD_3OD at ca. 25 ^oC with a 1:1.5 molar ratio of thioanisole versus oxygen source and 0.2 mol% catalyst at an initial substrate concentration of 0.25 M in the absence of H_2O and the mixture was stirred for 60 minutes. [b] Conversions (Conv), mass balance (Mb) and product ratios were determined by ^1H-NMR (JEOL 500M) or by quantitative GC-MS analysis with an internal standard (1,2,4-trichlorobenzene) on the crude reaction mixture after the reaction is quenched by sodium hydroxide solution (consuming all oxygen source).

4.3.3 Catalytic oxidation of substituted hydroxy and allylic sulfides by $PhI(OAc)_2$

Its efficacy for epoxidation was tested on *cis*-cyclooctene under the optimized reaction conditions. Remarkably, no epoxide was formed (<1% Conv.) was observed after 24 h under identical reaction conditions. This result stimulates us to test the oxidation of allylic sulfides. Table 11 lists the oxidized products and corresponding selectivities using the **4a** and **4b** as the catalyst, respectively. In analogy with what we observed for **6a**, all catalytic oxidation of substituted thioanisoles proceeded with a

quantitative conversion into the corresponding sulfoxides with excellent selectivity (100%) and mass balance (> 90%) in the short period of 60 minutes, and in all cases no sulfones were detected even in the presence of H_2O. With iron(III) catalyst and $PhI(OAc)_2$, no epoxidation took place and excellent chemoselectivities for sulfoxide were obtained (entry 1-2 and 6-7). Similarly, presence of hydroxy group did not disturb the selective oxidation of sulfide to sulfoxide and no alcohol oxidation was observed (entry 3-4 and 8-9). Notably, the catalytic oxidation of vinyl sulfides performed excellent chemoselectivities of sulfide to sulfoxide (entry 5 and 10).

Table 11. Catalytic oxidation of allylic or hydroxy sulfides by iron corrole (**4**) and $PhI(OAc)_2$[a].

Entry	Catalyst **4**	Substrate **6**	Product **7**	Conv (%)[b]	yield (%)[b]
1	$Fe^{III}(TPC)\cdot(OEt_2)_2$ **4a**	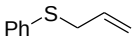	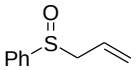	75 (78)[c]	100
2		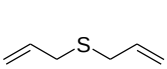	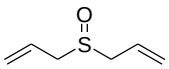	100	100
3		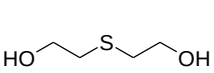	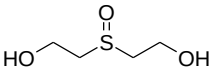	71 (100)[c]	100
4		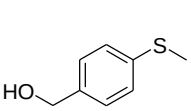	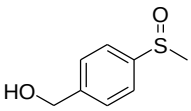	95	100
5		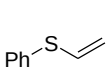	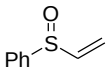	32 (100)[d]	100
6	$Fe^{III}(TPFC)\cdot(OEt_2)_2$ **4b**	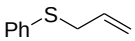	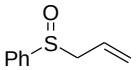	75 (75)[c]	100
7		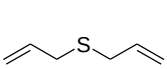	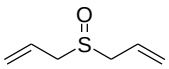	100	100
8		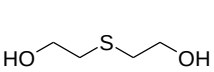	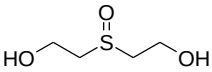	67 (100)[c]	100
9		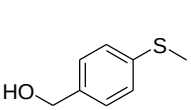	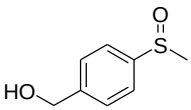	92	100
10[d]		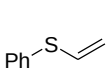	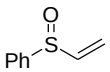	85	100

[a] Unless otherwise specified, all reactions were performed in CD_3OD (2 mL) at ca. 25 °C with 1.5 equiv. of $PhI(OAc)_2$ (0.75 mmol), substrate (0.5 mmol), 0.2 mol% catalyst in the absence of H_2O and the mixture was stirred for 60 minutes; only sulfoxide was detected by ^{1}H-NMR analysis of the crude reaction mixture.

[b] Based on the conversion of thioanisoles and determined by ^{1}H-NMR analysis of the crude reaction mixture; material balance > 95%. The products were fully characterized after column chromatography.

[c] 0.25 mmol of H_2O was used.

[d] 0.5 mmol of H_2O was used.

4.4 Mechanistic studies

We conducted the chemical oxidation reaction of iron(III) catalyst **4** with $PhI(OAc)_2$ in methanol in the absence of sulfides. As we noted, the coordinating solvent of methanol resulted in the change of UV-vis spectrum of $Fe^{III}(TPC)\cdot(OEt_2)_2$ (**4a**). The absorption spectrum shifted from twin peaks Soret band at 408 nm and broad absorption bands around 635 nm to single peak Soret band at 400 nm and broad absorption bands. The change of UV-vis spectrum in MeOH is presumably due to the ligand exchange on the metal center.[37] In the presence of excess $PhI(OAc)_2$, **4a** decayed steadily as shown in Figure 36. The later signal of the final product is still unknown. The mechanistic studies and transient oxidizing intermediates on iron(III) corrole (**4**) system are under investigation in our laboratory.

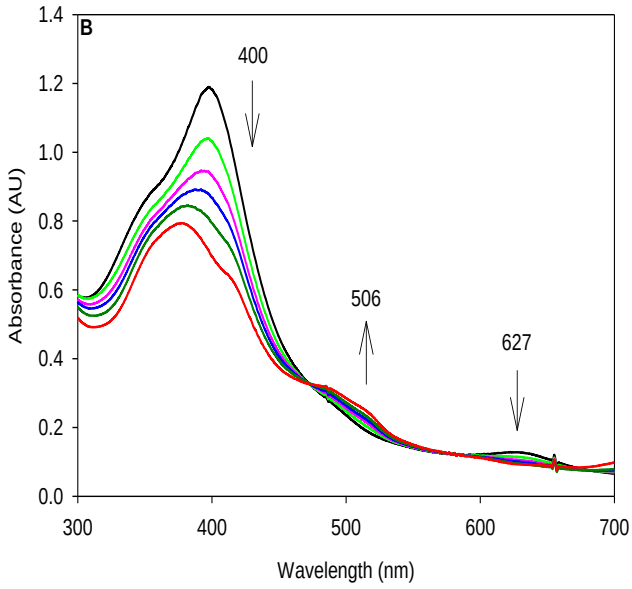

Figure 36. Time-resolved spectrum for the oxidation of **4a** (5×10^{-6} M) with 20 equivalent of $PhI(OAc)_2$ in CH_3OH.

5. CONCLUSIONS

An efficient method for the highly selective oxidation of sulfides to sulfoxides with ruthenium porphyrin as catalyst in the presence of $PhI(OAc)_2$ and visible light has been developed. All the factors that effected the catalytic sulfoxidation reactions were well investigated and understood. Various thioanisoles and allylic sulfides could be successfully oxidized with good conversions (most quantitative) and excellent selectivities. The observed catalytic oxidation is ascribed to the generation of low-reactivity ruthenium(IV)-oxo intermediate that can be directly observed by UV-vis spectroscopy. A plausible mechanism for the catalytic sulfoxidations by ruthenium catalyst and $PhI(OAc)_2$ has been proposed. Further studies to define synthetic applications and characterize the observed transients more fully are underway in our laboratory.

We have shown that a fluorinated diiron(IV)-μ-oxo biscorrole catalyzed aerobic oxidation of alkenes and activated hydrocarbons under visible light irradiation. The observed photocatalytic oxidation is ascribed to a photo-disproportionation mechanism to afford a highly reactive corrole-iron(V)-oxo species. It is noteworthy that the use of visible light (solar light) for activation of atmospheric oxygen without the consumption of a reducing agent in aforementioned photocatalysis is particularly relevant to realizing innovative and economically advantageous processes for conversion of hydrocarbons into oxygenates.

Iron(III) corroles was utilized for the highly selective sulfoxidation reactions with $PhI(OAc)_2$ as mild oxygen source. Various allylic thioanisoles and hydroxy sulfides have

been successfully oxidized to the corresponding sulfoxides with good conversions (most quantitative) and excellent selectivities. A significant water effect on the rate of sulfoxidation formation was observed. The probe of mechanism and characterization of transient iron-oxo corroles are under way in our laboratory.

REFERENCE

1. Ortiz de Montellano, P. R., *Cytochrome P450 Structure, Mechanism, and Biochemistry*. 3rd ed.; Kluwer Academic/Plenum: New York, 2005.

2. Sheldon, R. A., *Metalloprophyrins In Catalytic Oxidations*. Marcel Dekker: New York, 1994.

3. Brink, G. t., Green, Catalytic Oxidation of Alcohols in Water. *Science* **2000,** *287* (5458), 1636-1639.

4. Groves, J. T., Shalyaev, K.; Lee, J., Oxometalloporphyrins in Oxidative Catalysis. In *The Porhyrin Handbook,* Kadish, K. M. S., K. M.; Guilard, R., Ed. 2000; Vol. 4, pp 17-40.

5. Punniyamurthy, T.; Velusamy, S.; Iqbal, J., Recent Advances in Transition Metal Catalyzed Oxidation of Organic Substrates with Molecular Oxygen. *Chem.Rev.* **2005,** *105* (6), 2329-2363.

6. Zhang, R.; Vanover, E.; Chen, T.-H.; Thompson, H., Visible Light-Driven Aerobic Oxidation Catalyzed by a Diiron(IV) μ-oxo Biscorrole Complex. *Appl. Catal. A* **2013,** *465*, 95-100.

7. Zhang, R., Asymmetric Organic Oxidation by Chiral Ruthenium Complexes Containing D_2- and D_4- Symmetric Porphyrinato Ligands. *Ph. D. Thesis* **2000**, 1-235.

8. Sono, M.; Roach, M. P.; Coulter, E. D.; Dawson, J. H., Heme-Containing Oxygenases. *Chem. Rev.* **1996,** *96* (7), 2841-2887.

9. Denisov, I. G.; Makris, T. M.; Sligar, S. G.; Schlichting, I., Structure and Chemistry of Cytochrome P450. *Chem. Rev.* **2005,** *105* (6), 2253-2277.

10. Newcomb, M.; Zhang, R.; Chandrasena, R. E. P.; Halgrimson, J. A.; Horner, J. H.; Makris, T. M.; Sligar, S. G., Cytochrome P450 Compound I. *J. Am. Chem. Soc.* **2006,** *128* (14), 4580-4581.

11. Meunier, B., *Metal-Oxo and Metal-Peroxo Species in Catalytic Oxidations*. Springer-Verlag: Berlin, 2000.

12. Rui, L.; Pochapsky, S. S.; Pochapsky, T. C., Comparison of the Complexes Formed by Cytochrome $P450_{cam}$ with Cytochrome b_5 and Putidaredoxin, Two Effectors of Camphor Hydroxylase Activity. *Biochemistry* **2006,** *45*, 3887-3897.

13. Poulos, T. L.; Finzel, B. C.; Howard, A. J., Crystal Structure of Substrate-Free *Pseudomonas Putida* Cytochrome P450. *Biochemistry* **1986,** *25*, 5314-5322.

14. Poulos, T. L.; Finzel, B. C.; Howard, A. J., High-Resolution Crystal Structure of Cytochrome $P450_{cam}$. *J. Mol. Biol.* **1987,** *195*, 687-700.

15. Zhang, R.; Nagraj, N.; Lansakara-P, D. S. P.; Hager, L. P.; Newcomb, M., Kinetics of Two-Electron Oxidations by the Compound I Derivative of Chloroperoxidase, a Model for Cytochrome P450 Oxidants. *Org. Lett.* **2006,** *8* (13), 2731-2734.

16. Groves, J. T., Reactivity and Mechanisms of Metalloporphyrin-Catalyzed Oxidations. *J. Porph. Phthal.* **2000,** *4*, 350-352.

17. Meunier, B., Metalloporphyrins as Versatile Catalysts for Oxidation Reactions and Oxidative DNA Cleavage. *Chem. Rev.* **1992,** *92* (6), 1411-1456.

18. Che, C.-M.; Huang, J.-S., Metalloporphyrin-Based Oxidation Systems: from Biomimetic Reactions to Application in Organic Synthesis. *Chem. Commun.* **2009**, 3996-4015.

19. Groves, J. T.; Nemo, T. E.; Myers, R. S., Hydroxylation and Epoxidation Catalyzed by Iron-Porphine Complexes. Oxygen Transfer from Iodosylbenzene. *J. Am. Chem. Soc.* **1979,** *101*, 1032-1033.

20. Nam, W., High-Valent Iron(IV)–Oxo Complexes of Heme and Non-Heme Ligands in Oxygenation Reactions. *Acc. Chem. Res.* **2007,** *40*, 522-531.

21. Meunier, B.; Visser, S. l. P. d.; Shaik, S., Mechanism of Oxidation Reactions Catalyzed by Cytochrome P450 Enzymes. *Chem. Rev.* **2004,** *104*, 3947-3980.

22. Groves, J. T.; Lee, J.; Marla, S. S., Detection and Characterization of an Oxomanganese(V) Porphyrin Complex by Rapid-Mixing Stopped-Flow Spectrophotometry. *J. Am. Chem. Soc.* **1997,** *119* (27), 6269-6273.

23. Wang, C.; Shalyaev, K. V.; Bonchio, M.; Carofiglio, T.; Groves, J. T., Fast Catalytic Hydroxylation of Hydrocarbons with Ruthenium Porphyrins. *Inorg. Chem.* **2006,** *45* (12), 4769-4782.

24. Hodgkin, D. C.; Pickworth, J.; Robertson, J. H.; Trueblood, K. N.; Prosen, R. J.; White, J. G., Structure of Vitamin B_{12} : The Crystal Structure of the Hexacarboxylic Acid derived from B_{12} and the Molecular Structure of the Vitamin. *Nature* **1955,** *176*, 325-328.

25. Johnson, A. W.; Kay, I. T., 306. Corroles. Part I. Synthesis. *J. Chem. Soc.* **1965**, 1620-1629.

26. Grigg, R.; Hamilton, R. J.; Jozefowicz, M. L.; Rochester, C. H.; Terrell, R. J.; Wickwar, H., A Spectroscopic Study of the Protonation of Porphins and Corroles. *J. Chem. Soc., Perkin Trans.* **1973,** *407-413*.

27. Ghosh, A.; Steene, E., High-Valent Transition Metal Centers Versus Noninnocent Ligands in Metallocorroles: Insights from Electrochemistry and Implications for High-Valent Heme Protein Intermediates. *J. Inorg. Biochem.* **2002,** *91*, 423-436.

28. Visser, S. P. d.; Ogliaro, F.; Gross, Z.; Shaik, S., What Is the Difference between the Manganese Porphyrin and Corrole Analogues of Cytochrome P450's Compound I? *Chem. Eur. J.* **2001,** *7*, 4954-4960.

29. Gross, Z., High-Valent Corrole Metal Complexes. *J. Biol. Inorg. Chem.* **2001,** *6*, 733-738.

30. Koszarna, B. G., Gryko, D. T., Efficient Synthesis of Meso-Subsitutted Corroles in a H_2O-MeOH Mixture. *J. Org. Chem.* **2006,** *71*, 3707-3717.

31. Gross, Z.; Galili, N., *N*-Substituted Corroles: a Novel Class of Chiral Ligands. *Angew. Chem., Int. Ed. Engl.* **1999,** *38* (16), 2366-2369.

32. Gross, Z.; Galili, N.; Simkhovich, L.; Saltsman, I.; Botoshansky, M.; Blaeser, D.; Boese, R.; Goldberg, I., Solvent-Free Condensation of Pyrrole and Pentafluorobenzaldehyde: A Novel Synthetic Pathway to Corrole and Oligopyrromethenes. *Org. Lett.* **1999,** *1* (4), 599-602.

33. Harrison, H. R.; Hodder, O. J. R.; Hodgkin, D. C., Crystal and Molecular Structure of 8,12-Diethyl-2,3,7,13,17,18-hexamethylcorrole. *J. Chem. Soc. B* **1971**, 640-645.

34. Gryko, D. T., Recent Advances in the Synthesis of Corroles and Core-Modified Corroles. *Eur. J. Org. Chem.* **2002**, 1735-1743.

35. Ghosh, A., A Perspective of One-Pot Pyrrole-Aldehyde Condensations as Versatile Self-Assembly Processes. *Angew. Chem. Int. Ed.* **2004,** *43* (15), 1918-1931.

36. Gross, Z.; Gray, H. B., Oxidations Catalyzed by Metallocorroles. *Adv. Syn. Catal.* **2004,** *346* (2+3), 165-170.

37. Aviv, I.; Gross, Z., Corrole-Based Applications. *Chem. Commun.* **2007,** (20), 1987-1999.

38. Gross, Z.; Gray, H. B., How Do Corroles Stabilize High Valent Metals? *Comments Inorg. Chem.* **2006,** *27* (3-4), 61-72.

39. Gross, Z.; Simkhovich, L.; Galili, N., First Catalysis by Corrole Metal Complexes: Epoxidation, Hydroxylation, and Cyclopropanation. *Chem. Commun.* **1999**, 599-600.

40. Ogliaro, F., de Visser, S. P., Groves, J. T., and Shaik, S., Chameleon States: High-Valent Metal-Oxo Species of Cytochrome P450 and Its Ruthenium Analogue. *Angew. Chem. Int. Ed.* **2001,** *40*, 2874-2878.

41. Zhang, R.; Horner, J. H.; Newcomb, M., Laser Flash Photolysis Generation and Kinetic Studies of Porphyrin-Manganese-Oxo Intermediates. Rate Constants for Oxidations Effected by Porphyrin-Mn^{V}-Oxo Species and Apparent Disproportionation

Equilibrium Constants for Porphyrin-Mn^{IV}-Oxo Species. *J. Am. Chem. Soc.* **2005,** *127* (18), 6573-6582.

42. Zhang, R.; Newcomb, M., Laser Flash Photolysis Formation and Direct Kinetic Studies of Manganese(V)-Oxo Porphyrin Intermediates. *J. Am. Chem. Soc.* **2003,** *125* (41), 12418-12419.

43. Tiago de Oliveira, F.; Chanda, A.; Banerjee, D.; Shan, X.; Mondal, S.; Que, L., Jr.; Bominaar, E. L.; Muenck, E.; Collins, T. J., Chemical and Spectroscopic Evidence for an Fe^{V}-Oxo Complex. *Science* **2007,** *315* (5813), 835-838.

44. Harischandra, D. N.; Zhang, R.; Newcomb, M., Photochemical Generation of a Highly Reactive Iron-Oxo Intermediate. A True Iron(V)-Oxo Species? *J. Am. Chem. Soc.* **2005,** *127* (40), 13776-13777.

45. Pan, Z.; Zhang, R.; Fung, L. W. M.; Newcomb, M., Photochemical Production of a Highly Reactive Porphyrin-Iron-Oxo Species. *Inorg. Chem.* **2007,** *46* (5), 1517-1519.

46. Kowalski, P.; Mitka, K.; Ossowska, K.; Kolarska, Z., Oxidation of Sulfides to Sulfoxides. Part 1: Oxidation Using Halogens Derivatives. *Tetrahedron* **2005,** *61*, 1933-1953.

47. Caron, S.; Dugger, R. W.; Ruggeri, S. G.; Ragan, J. A.; Ripin, D. H. B., Large-Scale Oxidations in the Pharmaceutical Industry. *Chem. Rev.* **2006,** *106*, 2943-2989.

48. Baeckvall, J. E., *Modern oxidation methods*. Wiley-VCH Verlag: Weinheim, 2004.

49. Wojaczynska, E. W., J., Enantioselective Synthesis of Sulfoxides: 2000-2009. *Chem. Rev.* **2010,** *110*, 4303-4356.

50. Hosseinpoor, F.; Golchoubian, H., Mn(III)-Catalyzed Oxidation of Sulfides to Sulfoxides with Hydrogen Peroxide. *Tetrahedron Lett.* **2006,** *47* (29), 5195-5197.

51. Kaczorowska, K.; Kolarska, Z.; Mitka, K.; Kowalski, P., Oxidation of Sulfides to Sulfoxides. Part 2: Oxidation by Hydrogen Peroxide. *Tetrahedron* **2005,** *61* (35), 8315-8327.

52. Surendra, K.; Krishnaveni, N. S.; Kumar, V. P.; Sridhar, R.; Rao, K. R., Selective and Efficient Oxidation of Sulfides to Sulfoxides with *N*-Bromosuccinimide in the Presence of *β*-Cyclodextrinin Water. *Tetrahedron Lett.* **2005,** *46* (27), 4581-4583.

53. Chellamani, A.; Alhaji, N. I.; Rajagopal, S., Kinetics and Mechanism of (salen)Mn^{III}–Catalysed Hydrogen Peroxide Oxidation of Alkyl Aryl Sulphides. *J. Phys. Org. Chem.* **2007,** *20* (4), 255-263.

54. Sevvel, R.; Rajagopal, S.; Srinivasan, C.; Alhaji, I. N.; Chellamani, A., Mechanism of Selective Oxidation of Organic Sulfides with Oxo(salen)chromium(V) Complexes. *J. Org. Chem.* **2000,** *65*, 3334-3340.

55. Leung, W. H.; Che, C. M., High-Valent Ruthenium(IV) and -(VI) Oxo Complexes of Octaethylporphyrin. Synthesis, Spectroscopy, and Reactivities. *J. Am. Chem. Soc.* **1989,** *111* (24), 8812-8818.

56. Lindsey, J. S.; Wagner, R. W., Investigation of the Synthesis of *ortho*-Substituted Tetraphenylporphyrins. *J. Org. Chem.* **1989,** *54*, 828-836.

57. Che, C.-M.; Zhang, J.-L.; Zhang, R.; Huang, J.-S.; Lai, T.-S.; Tsui, W.-M.; Zhou, X.-G.; Zhou, Z.-Y.; Zhu, N.; Chang, C. K., Hydrocarbon Oxidation by *beta*-Halogenated Dioxoruthenium(VI) Porphyrin Complexes: Effect of Reduction Potential ($Ru^{VI/V}$) and C-H Bond-Dissociation Energy on Rate Constants. *Chem. Eur. J* **2005,** *11* (23), 7040-7053.

58. Gross, Z.; Galili, N.; Saltsman, I., The First Direct Synthesis of Corroles from Pyrrole. *Angew. Chem. Int. Ed.* **1999,** *38*, 1427-1429.

59. Paolesse, R.; Nardis, S.; Sagone, F.; Khoury, R. G., Synthesis and Functionalization of *meso*-Aryl-Substituted Corroles. *J. Org. Chem.* **2001,** *66*, 550-556.

60. Simkhovich, L.; Galili, N.; Saltsman, I.; Goldberg, I.; Gross, Z., Coordination Chemistry of the Novel 5,10,15-Tris(pentafluorophenyl)corrole: Synthesis, Spectroscopy, and Structural Characterization of Its Cobalt(III), Rhodium(III), and Iron(IV) Complexes. *Inorg. Chem.* **2000,** *39*, 2704-2705.

61. Simkhovich, L.; Mahammed, A.; Goldberg, I.; Gross, Z., Synthesis and Characterization of Germanium, Tin, Phosphorus, Iron, and Rhodium Complexes of Tris(pentafluorophenyl)corrole, and the Utilization of the Iron and Rhodium Corroles as Cyclopropanation Catalysts. *Chem. Eur. J.* **2001,** *7* (5), 1041-1055.

62. Zhang, R.; Huang, Y.; Abebrese, C.; Thompson, H.; Vanover, E.; Webb, C., Generation of *trans*-Dioxoruthenium(VI) Porphyrins: A Photochemical Approach. *Inorg. Chim. Acta* **2011,** *372*, 152-157.

63. Che, C.-M.; Yu, W.-Y., Ruthenium-Oxo and -Tosylimido Porphyrin Complexes for Epoxidation and Aziridination of Alkenes. *Pure Appl. Chem.* **1999,** *71* (2), 281-288.

64. Nam, W.; Lim, M. H.; Moon, S. K.; Kim, C., Participation of Two Distinct Hydroxylating Intermediates in Iron(III) Porphyrin Complex-Catalyzed Hydroxylation of Alkanes. *J. Am. Chem. Soc.* **2000,** *122* (44), 10805-10809.

65. Ohtake, H.; Higuchi, T.; Hirobe, M., The Highly Efficient Oxidation of Olefins, Alcohols, Sulfides and Alkanes with Heteroaromatic *N*-Oxides Catalyzed by Ruthenium Porphyrins. *Heterocycles* **1995,** *40* (2), 867-903.

66. Rajapakse, N.; James, B. R.; Dolphin, D., Catalytic O_2-Oxidation of Thioethers to Sulfoxides Using Ruthenium(VI) Dioxo Porphyrin Species. *Catal. Lett.* **1989,** *2*, 219-226.

67. Collman, J. P.; Chien, A. S.; Eberspacher, T. A.; Brauman, J. I., Multiple Active Oxidants in Cytochrome P-450 Model Oxidations. *J. Am. Chem. Soc.* **2000,** *122* (45), 11098-11100.

68. In, J.-H.; Park, S.-E.; Song, R.; Nam, W., Iodobenzene Diacetate as an Efficient Terminal Oxidant in Iron(III) Porphyrin Complex-Catalyzed Oxygenation Reactions. *Inorg. Chim.Acta* **2003,** *343*, 373-376.

69. Adam, W.; Hajra, S.; Herderich, M.; Saha-Moller, C. R., A Highly Chemoselective Oxidation of Alcohols to Carbonyl Products with Iodosobenzene Diacetate Mediated by Chromium(III)(salen) Complexes: Synthetic and Mechanistic Aspects. *Org. Lett.* **2000,** *2*, 2773-2776.

70. Nishiyama, H.; Motoyama, Y., Novel Ruthenium–Pyridinedicarboxylate Complexes of Terpyridine and Chiral Bis(Oxazolinyl)Pyridine: a new Catalytic System

for Alkene Epoxidation with [Bis(Acetoxy)Iodo]Benzene as an Oxygen Donor. *Chem. Commun.* **1997**, 1863-1864.

71. Hoshino, M.; Kashiwagi, Y., Photoinduced Decarbonylation of Ruthenium(II) Carbonyl Octaethylporphyrin in Acetonitrile: Studies on the Origin of the Excitation Wavelength Dependence. *J. Phys. Chem.* **1990,** *94*, 673-678.

72. Groves, J. T.; Quinn, R., Models of Oxidized Heme Proteins. Preparation and Characterization of a *trans*-Dioxoruthenium(VI) Porphyrin Complex. *Inorg. Chem.* **1984,** *23* (24), 3844-38466.

73. Abebrese, C.; Huang, Y.; Pan, A.; Yuan, Z.; Zhang, R., Kinetic Studies of oxygen Atom Transfer Reactions from *trans*-Dioxoruthenium(VI) Porphyrins to Sulfides. *J. Inorg. Biochem.* **2011,** *105*, 1555-1561.

74. Zhang, R.; Newcomb, M., Laser Flash Photolysis Generation of High-Valent Transition Metal-Oxo Species: Insights from Kinetic Studies in Real Time. *Acc.Chem. Res.* **2008,** *41* (3), 468-477.

75. Pan, Z.; Zhang, R.; Newcomb, M., Kinetic Studies of Reactions of Iron(IV)-Oxo Porphyrin Radical Cations with Organic Reductants. *J. Inorg. Biochem.* **2006,** *100* (4), 524-532.

76. Watanabe, Y.; Fujii, H., Characterization of High-Valent Oxo-Metalloporphyrins. In *Metal-Oxo and Metal-Peroxo Species in Catalytic Oxidations*, Meunier, B., Ed. Springer-Verlag: Berlin, 2000.

77. Maldotti, A.; Molinari, A.; Amadelli, R. , Photocatalysis with Organized Systems for the Oxofunctionalization of Hydrocarbons by O_2. *Chem. Rev.* **2002,** *102*, 3811-3836.

78. Collman, J. P.; Wagenknecht, P. S.; Hutchison, J. E., Cofacial Bis(Metallo)Diporphyrins as Potential Molecular Catalysts for Multielectron Reductions and Oxidations of Small Molecules. *Angew. Chem.* **1994,** *106* (15/16), 1620-39.

79. Rosenthal, J.; Bachman, J.; Dempsey, J. L.; Esswein, A. J.; Gray, T. G.; Hodgkiss, J. M.; Manke, D. R.; Luckett, T. D.; Pistorio, B. J.; Veige, A. S.; Nocera, D. G., Oxygen and Hydrogen Photocatalysis by Two-Electron Mixed-Valence Coordination Compounds. *Coord. Chem. Rev.* **2005,** *249* (13-14), 1316-1326.

80. Peterson, M. W.; Rivers, D. S.; Richman, R. M., Mechanistic Considerations in the Photodisproportionation of μ-Oxo-bis((tetraphenylporphinato)iron(III)). *J. Am. Chem. Soc.* **1985,** *107* (10), 2907-15.

81. Wasser, I. M.; Fry, H. C.; Hoertz, P. G.; Meyer, G. J.; Karlin, K. D., Photochemical Organic Oxidations and Dechlorinations with a μ-Oxo Bridged Heme/Non-Heme Diiron Complex. *Inorg. Chem.* **2004,** *43* (26), 8272-8281.

82. Vanover, E.; Huang, Y.; Xu, L.; Newcomb, M.; Zhang, R., Photocatalytic Aerobic Oxidation by a Bis-porphyrin-ruthenium(VI) μ-Oxo Dimer: Observation of a Putative Porphyrin-Ruthenium(V)-Oxo Intermediate. *Org. Lett.* **2010,** *12*, 2246-2249.

83. Harischandra, D. N.; Lowery, G.; Zhang, R.; Newcomb, M., Production of a Putative Iron(V)−Oxo Corrole Species by Photo-Disproportionation of a Bis-Corrole-

Diiron(IV)-μ-Oxo Dimer: Implication for a Green Oxidation Catalyst. *Org. Lett.* **2009,** *11*, 2089-2092.

84. Simkhovich, L.; Goldberg, I.; Gross, Z., Iron(III) and Iron(IV) Corroles: Synthesis, Spectroscopy, Structures, and No Indications for Corrole Radicals. *Inorg. Chem.* **2002,** *41* (21), 5433-5439.

85. Rosenthal, J.; Pistorio, B. J.; Chng, L. L.; Nocera, D. G., Aerobic Catalytic Photooxidation of Olefins by an Electron-Deficient Pacman Bisiron(III) μ-Oxo Porphyrin. *J. Org. Chem.* **2005,** *70* (5), 1885-1888.

86. In, J.-H.; Park, S.-E.; Song, R.; Nam, W., Iodobenzene Diacetate as an Efficient Terminal Oxidant in Iron(III) Porphyrin Complex-Catalyzed Oxygenation Reactions. *Inorg. Chim. Acta* **2003,** *343*, 373-376.

CURRICULUM VITAE

Articles in peer-reviewed journals

1. Zhang, R.; Vanover, E.; Chen, T.-H.; Thompson, H., Visible Light-Driven Aerobic Oxidation Catalyzed by a Diiron(IV) μ-Oxo Biscorrole Complex. *Appl. Catal. A* **2013,** *465*, 95-100.

2. Chen, T.-H.; Yuan, Z.; Carver, A.; Zhang, R., Visible Light-Promoted Selective Oxidation of Sulfides to Sulfoxides Catalyzed by Ruthenium Porphyrins with Iodobenzene Diacetate. *Appl. Catal. A* **2014** (ASAP Article).

Presentations at academic conferences

1. Chen, T.-H.; Vanover, E.; Huang, Y.; Zhang, R. "Photocatalytic Aerobic Oxidation by Highly Reactive Metal-Oxo Species with Visible Light." NSF EPSCoR, Nashville, TN, November 2013.

2. Chen, T.-H.; Vanover, E.; Thompson, H.; Zhang, R. "Visible Light-Driven Aerobic Oxidation Catalyzed by a Diiron(IV) μ-Oxo Biscorrole Complex." Kentucky Academy of Science, Morehead, Ky, November 2013.

3. Chen, T.-H.; Vanover, E.; Thompson, H.; Zhang, R. "Visible Light-Driven Aerobic Oxidation Catalyzed by a Diiron(IV) μ-Oxo Biscorrole Complex." WKU Student Research Conference, Bowling Green, Ky, March 2013.

4. Chen, T.-H.; Yuan Z.; Zhang, R. "Synthesis and Characterization of Corroles and Iron(III) Corroles." Kentucky Academy of Science, Richmond, Ky, October 2012.

ABBREVIATIONS AND SYMBOLS

2,6-Cl_2PyNO	2,6-dichloropyridine *N*-oxide
$BF_3 \cdot OEt_2$	Boron trifluoride diethyl etherate
DDQ	2,3-Dichloro-5,6-dicyano-*p*-benzequinone
DMF	*N*,*N*-Dimethylformamide
FID	Flame ionization detector
$Fe^{III}(Cor) \cdot (OEt)_2$	Iron(III) corrole complexes
$Fe^{III}(TPC) \cdot (OEt)_2$	Iron(III) 5,10,15-triphenylcorrole
$Fe^{III}(TNPC) \cdot (OEt)_2$	Iron(III) 5,10,15-tris(4-nitrophenyl)corrole
$Fe^{III}(TPFC) \cdot (OEt)_2$	Iron(III) 5,10,15-tri(pentafluorophenyl)corrole
$[Fe^{IV}(TPFC)]_2O$	diiron(IV) μ-oxo biscorrole
GC	Gas chromatograph
^{1}H-NMR	Proton nuclear magnetic resonance
H_2TMP	*meso*-Tetramesitylporphyrin
H_2TPFPP	*meso*-Tetrakis(5,10,15,20-pentafluorophenyl)porphyrin
H_3Cor	*meso*-Triphenylcorrole
H_3TPC	5,10,15-Triphenylcorrole
H_3TNPC	5,10,15-Tris(4-nitrophenyl)corrole
H_3TPFC	5,10,15-Tri(pentafluorophenyl)corrole
k_2	Second-order rate constant
k_{obs}	Observed pseudo-first-order rate constant
k_{rel}	Relative rate constant
m-CPBA	*meta*-Chloroperoxybenzoic acid

MS	Mass spectroscopy
PhIO	Iodosylbenzene
$PhI(OAc)_2$	Iodobenzene diacetate
$Ru_3(CO)_{12}$	Triruthenium dodecacarbonyl
Ru^{II}(Por)(CO)	Ruthenium(II) carbonyl porphyrin complex
Ru^{II}(TMP)(CO)	Ruthenium(II) carbonyl (5,10,15,20-tetramesitylporphyrinato)
Ru^{II}(TPFPP)(CO)	Ruthenium(II) carbonyl [5,10,15,20-tetrakis(pentafluorophenyl)porphyrinato]
$Ru^{VI}(TMP)O_2$	*trans*-Dioxo(5,10,15,20-tetramesitylporphyrinato) ruthenium(VI)
TBHP	*tert*-Butyl hydroperoxide
TONs	Turnover numbers
UV-vis	Ultraviolet-visible